Near-Surface Water Balance of an Undeveloped Upland Site in West-Central Florida

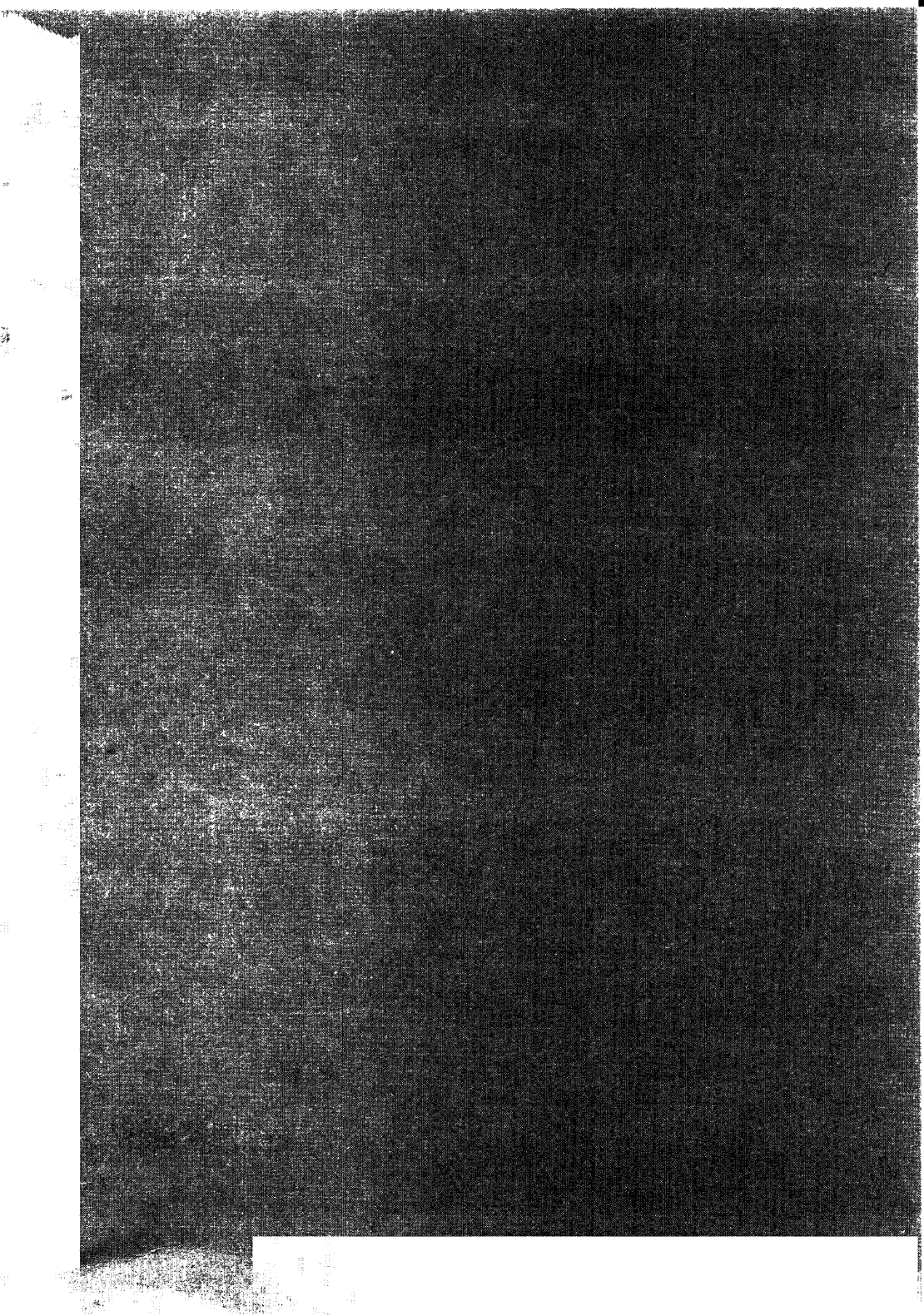

United States Geological Survey Water-Supply Paper 2452

Prepared in cooperation with the Florida Water Management District, and Sarasota County, Florida

AVAILABILITY OF BOOKS AND MAPS OF THE U.S. GEOLOGICAL SURVEY

Instructions on ordering publications of the U.S. Geological Survey, along with prices of the last offerings, are given in the current-year issues of the monthly catalog "New Publications of the U.S. Geological Survey." Prices of available U.S. Geological Survey publications released prior to the current year are listed in the most recent annual "Price and Availability List." Publications that may be listed in various U.S. Geological Survey catalogs (**see back inside cover**) but not listed in the most recent annual "Price and Availability List" may be no longer available.

Order U.S. Geological Survey publications **by mail** or **over the counter** from the offices given below.

BY MAIL

Books

Professional Papers, Bulletins, Water-Supply Papers, Techniques of Water-Resources Investigations, Circulars, publications of general interest (such as leaflets, pamphlets, booklets), single copies of Preliminary Determination of Epicenters, and some miscellaneous reports, including some of the foregoing series that have gone out of print at the Superintendent of Documents, are obtainable by mail from

U.S. Geological Survey, Information Services
Box 25286, Federal Center, Denver, CO 80225

Subscriptions to Preliminary Determination of Epicenters can be obtained ONLY from the

Superintendent of Documents
Government Printing Office
Washington, DC 20402

(Check or money order must be payable to Superintendent of Documents.)

Maps

For maps, address mail orders to

U.S. Geological Survey, Information Services
Box 25286, Federal Center, Denver, CO 80225

OVER THE COUNTER

Books and Maps

Books and maps of the U.S. Geological Survey are available over the counter at the following U.S. Geological Survey Earth Science Information Centers (ESIC's), all of which are authorized agents of the Superintendent of Documents:

- **ANCHORAGE, Alaska**—Rm. 101, 4230 University Dr.
- **LAKEWOOD, Colorado**—Federal Center, Bldg. 810
- **MENLO PARK, California**—Bldg. 3, Rm. 3128, 345 Middlefield Rd.
- **RESTON, Virginia**—USGS National Center, Rm. 1C402, 12201 Sunrise Valley Dr.
- **SALT LAKE CITY, Utah**—Federal Bldg., Rm. 8105, 125 South State St.
- **SPOKANE, Washington**—U.S. Post Office Bldg., Rm. 135, West 904 Riverside Ave.
- **WASHINGTON, D.C.**—Main Interior Bldg., Rm. 2650, 18th and C Sts., NW.

Maps Only

Maps may be purchased over the counter at the following U.S. Geological Survey offices:

- **ROLLA, Missouri**—1400 Independence Rd.
- **STENNIS SPACE CENTER, Mississippi**—Bldg. 3101

Near-Surface Water Balance of an Undeveloped Upland Site in West-Central Florida

By W.R. BIDLAKE and P.F. BOETCHER

Prepared in cooperation with the
Southwest Florida Water Management District, and
Sarasota County, Florida

U.S. Geological Survey Water-Supply Paper 2452

U.S. DEPARTMENT OF THE INTERIOR
BRUCE BABBITT, Secretary

U.S. GEOLOGICAL SURVEY
Gordon P. Eaton, Director

UNITED STATES GOVERNMENT PRINTING OFFICE, WASHINGTON: 1996

For sale by the
U.S. Geological Survey
Branch of Information Services
Box 25286
Federal Center
Denver, CO 80225–0286

Library of Congress Cataloging in Publication Data

Bidlake, W.R.
Near-surface water balance of an undeveloped upland site in West-Central Florida / by W.R. Bidlake and P.F. Boetcher.
46 p. cm.— (U.S. Geological Survey water-supply paper ; 2452)
"Prepared in cooperation with the Southwest Florida Water Management District and Sarasota County, Florida".
Includes bibliographical references (p.).
1.Water balance (Hydrology)—Florida. I. Boetcher, P.F.
II. Southwest Florida Water Management District. III. Series
GB705.F5B53 1997
551.49'09759—dc20 96–42200
CIP
ISBN 0–607–86212–2

CONTENTS

Abstract 1
Introduction 2
Purpose and Scope 2
Description of Study Area 3
Vegetation and Soils 5
Description of Near-Surface Water-Balance Components 5
Techniques and Instrumentation Used to Estimate Evapotranspiration and Potential Evapotranspiration 6
Energy-Balance Bowen Ratio 7
Energy-Balance Wind and Scalar Profile 11
Eddy Correlation 12
Estimation of Surface Roughness Parameters 13
Approaches for Estimating Daily Evapotranspiration 14
Penman Technique for Potential Evapotranspiration 15
Precipitation Measurement 16
Calibration of a Tipping-Bucket Rain Gage 16
Measurement of Soil-Water Content 18
Techniques for Estimating Vertical Water Flow 20
Computation of the Difference Between Surface-Water and Ground-Water Inflow and Outflow 21
Evapotranspiration and Apparent Potential Evapotranspiration 21
EBBR-EBWSP Approach 22
Eddy Correlation 30
Evapotranspiration Error 33
Apparent Potential Evapotranspiration 35
Precipitation 36
Soil-Water Content and Soil-Water Storage 37
Vertical Water Flow 39
Near-Surface Water Balance 40
Water Yield Error 43
Summary and Conclusions 43
References Cited 45

FIGURES

1. Map showing location of study area and study site on the T. Mabry Carlton, Jr., Memorial Reserve, Sarasota County, west-central Florida 4

2-22. Graphs showing:

2. Relation between vapor pressure determined using a dewpoint hygrometer and vapor pressure determined using a wet-bulb and dry-bulb psychrometer 10
3. Relation between gage calibration factor and simulated precipitation intensity for a tipping-bucket rain gage 17
4. Total precipitation measured at the study site from June 16, 1991, to January 16, 1992, by precipitation intensity class 18
5. Relation between volumetric soil-water content determined using core samples and the ratio of measurement and standard counts obtained with a neutron moisture gage 19
6. Energy fluxes estimated in conjunction with the energy-balance Bowen ratio and energy-balance wind and scalar profile techniques for January 14, 1992, and June 19, 1992 22

7. Latent heat flux estimated using the energy-balance Bowen ratio and energy-balance wind and scalar profile techniques for January 14, 1992 and June 19, 1992 24
8. Energy fluxes estimated in conjunction with eddy-correlation measurements on May 20, 1992 30
9. Energy-balance closure observed with eddy-correlation measurements as it varied with wind direction 32
10. Energy-balance closure observed with eddy-correlation measurements as it varied with time of day 32
11. Relation between daily evapotranspiration estimated using eddy correlation and daily evapotranspiration estimated using the energy-balance Bowen ratio and energy-balance wind and scalar profile techniques 33
12. Daily evapotranspiration estimated using eddy correlation as it varied with daily apparent potential evapotranspiration computed using the Penman equation 35
13. Latent heat flux represented by apparent potential evapotranspiration on May 20, 1992 36
14. Monthly precipitation at the study site, June 1991 through October 1992 36
15. Relation between precipitation measured using an accumulating rain gage and precipitation measured using a tipping-bucket rain gage 37
16. Volumetric soil-water content as it varied with depth on three dates 37
17. Relation between soil-water storage and depth to the water table 38
18. Relation between average volumetric soil-water content in the unsaturated zone and depth to the water table 38
19. Water-surface altitude in two monitor wells that were open to ground water at different depth intervals 39
20. Relation between water-surface altitude in a monitor well open to ground water over the depth interval of 0.3 to 3.4 meters and water-surface altitude in a piezometer open to ground water at a depth of 3.4 meters 39
21. Components of the near-surface water balance 41
22. Water yield and computed error in water yield caused by error in determining the rate of soil-water storage 43

TABLES

1. Roughness parameters d and z_0 and relation between sensible heat flux estimated using eddy correlation and sensible heat flux estimated using equation 8 14
2. Identification, relative location, and screened interval of monitor wells and piezometers in the study area 21
3. Energy-balance terms estimated in conjunction with energy-balance Bowen ratio and energy-balance wind and scalar profile techniques and summed over 24-hour and daytime periods for the dry prairie study site 23
4. Daily equivalent available energy, evapotranspiration, and apparent potential evapotranspiration 24
5. Energy fluxes and energy-balance closure estimated for 24-hour periods in conjunction with eddy-correlation measurements 31
6. Effect of thermocouple wire diameter and orientation of thermocouple support arms on the difference in air temperature measured over uniform vertical intervals with two presumably identical thermocouple pairs, and corresponding effects on evapotranspiration computed using the energy-balance Bowen ratio and the energy-balance wind and scalar profile techniques 34
7. Effect of changes in three time-series variables on evapotranspiration computed by the energy-balance Bowen ratio and the energy-balance wind and scalar profile techniques 34
8. Textural and structural characteristics and estimated saturated hydraulic conductivity of soil and sediment samples collected from a single soil profile 40
9. Components of the site water balance as integrated for different time periods 41

CONVERSION FACTORS, VERTICAL DATUM, ABBREVIATIONS, AND SYMBOLS

CONVERSION FACTORS

Multiply	by	To obtain
centimeter (cm)	0.3937	inch (in.)
cubic meter (m^3)	35.31	cubic foot
degree Celsius (°C)	1.8 × °C+32	degree Fahrenheit
degree Celsius per volt (°C/v)	1.8 × °C+32	degree Fahrenheit per volt
gram (g)	0.002205	pound mass
gram per cubic centimeter (g/cm^3)	0.03613	pound per cubic inch
gram per cubic meter (g/m^3)	0.00006243	pound per cubic foot
hectare (ha)	2.471	acre
joule per gram (J/g)	0.2388	calorie per gram
kilometer (km)	0.6214	mile
kilopascal (kPa)	0.2953	inch of mercury
	0.1450	pound per square inch
	10.00	millibar
megagram per cubic meter (Mg/m^3)	62.45	pound per cubic foot
megajoule per square meter per day ($MJ/m^2 \cdot d$)	11.57	watt per square meter
meter (m)	3.281	foot
meter per second (m/s)	283,500	foot per day
meter squared per second (m^2/s)	10.76	foot squared per second
millimeter (mm)	0.03937	inch
millimeter per day (mm/d)	0.03937	inch per day
millimeter per hour (mm/h)	0.03937	inch per hour
square kilometer (km^2)	0.3861	square mile (mi^2)
watt per square meter (W/m^2)	0.001433	calorie per square centimeter per minute

VERTICAL DATUM

Sea Level: In this report, "sea level refers to the National Geodetic Vertical Datum of 1929—a geodetic datum derived from a general adjustment of the first-order level nets of both the United States and Canada, formerly called Sea Level Datum of 1929.

Some conversion factors have assumed values for gravitational acceleration and density of water of 9.8 m/s^2 and 1.000 Mg/m^3, respectively, and are therefore only approximate.

ABBREVIATIONS

ch-co	chromel-constantan
EBBR	energy-balance Bowen ratio
EBWSP	energy-balance wind and scalar profile
Hz	hertz
PVC	polyvinylchloride
in.	inch
mi^2	square mile

Symbol	Meaning	Dimensions
a	Regression coefficient	dimensionless
b	Empirical parameter related to soil texture or regression coefficient	dimensionless
C	Energy-balance closure error	dimensionless
C_p	Specific heat of air at constant pressure	J/g •°C or J/g • kelvin
C_s	Specific heat of soil particles	J/g •°C
C_v	Factor to convert water flux to millimeters per day	mm s/m • d
C_w	Specific heat of water	J/g •°C
D	Depth of the water table	m
D_0	Vertical thickness of soil column	mm
d	Zero plane displacement height	m
E	Evapotranspiration	g/m^2 • s or mm/d
E_p	Potential evapotranspiration	g/m^2 • s or mm/d
$E_p^{'}$	Apparent potential evapotranspiration	g/m^2 • s or mm/d
e	Vapor pressure	kPa
e_s	Saturation vapor pressure	kPa
f	Neutron moisture gage count ratio	dimensionless
G	Subsurface heat flux	W/m^2
G_z	Subsurface heat flux at a fixed depth	W/m^2
g	Gravitational acceleration	m/s^2
H	Sensible heat flux	W/m^2
h	Hydraulic head	m
h_c	Height of plant canopy	m
h_g	Gravitational head	m
h_p	Pressure head	m
h_Ω	Overburden head	m
K_h	Eddy diffusivity for heat	m^2/s
K_v	Eddy diffusivity for water vapor	m^2/s
k	von Karman constant	dimensionless
k_{si}	Saturated hydraulic conductivity of a soil layer	m/s
$\bar{k}_s$	Effective saturated hydraulic conductivity	m/s

Symbol	Meaning	Dimensions
L	Obukhov stability length	m
M_w, M_d	Wet and dry mass of a soil core sample	g
m_c, m_s	Mass fractions of clay and silt	dimensionless
n	Sample size	dimensionless
P	Precipitation	mm/d
p	Total atmospheric pressure	kPa
q_d	Vertical water flow	mm/d
q_{ri}, q_{ro}	Lateral surface-water inflow and outflow	mm/d
q_{si}, q_{so}	Lateral ground-water inflow and outflow	mm/d
R_n	Net radiation	W/m^2
R_n^*	Unadjusted net radiation	W/m^2
r	Correlation coefficient	dimensionless
r_h	Aerodynamic resistance to heat transport	s/m
r^2	Coefficient of determination	dimensionless
S	Slope of the saturation vapor-pressure function	kPa/°C
$S_{y \cdot x}$	Standard error of estimate	dependent
S_θ	Soil-water storage	mm
T	Air temperature	°C
T_k	Absolute temperature	kelvins
t	Time	s
u	Horizontal wind speed	m/s
u^*	Friction velocity	m/s
V	Sample volume	m^3
w	Vertical wind speed	m/s
z	Soil depth or height above land surface	m
z_h	Roughness length for heat transport	m
z_0	Roughness length for momentum transport	m
z_0	Height at which wind speed is measured	m
β	Bowen ratio	dimensionless
γ	Psychrometer coefficient	kPa/°C
Δe	Spatial vapor pressure difference	kPa
Δh	Spatial hydraulic head difference	m

Symbol	Meaning	Dimensions
ΔS_θ	Change in soil-water storage	mm
ΔT	Spatial air temperature difference	°C
ΔT_s	Temporal change in soil temperature	°C
Δt	Duration of an averaging period	s
Δz	Length of a vertical interval	m
$\Delta\theta$	Spatial potential temperature difference	kelvins
ε	Ratio of molecular mass of water to that of dry air	dimensionless
θ	Volumetric water content	dimensionless

Symbol	Meaning	Dimensions
ρ_a	Air density	g/m^3
ρ_b	Soil bulk density	g/m^3
ρ_v	Water-vapor density	g/m^3
ρ_w	Water density	g/m^3
λ	Heat of vaporization for water	J/g
Ψ_h	Diabatic profile correction function for heat	dimensionless
Ψ_m	Diabatic profile correction function for momentum	dimensionless
$'$	Operator for momentary fluctuation from the mean	
$\overline{\quad}$	Operator for time average	

Near-Surface Water Balance of an Undeveloped Upland Site in West-Central Florida

By W.R. Bidlake *and* P.F. Boetcher

Abstract

Quantitative description of water balances of wildland ecosystems provides information that is useful in management of water and other resources of those systems. The near-surface water balance of a homogeneous area of wildland vegetation in west-central Florida was described quantitatively for June 1991 to October 1992. The study area was in the dry prairie vegetation type common to central Florida. The water balance was defined on a unit area basis for a depth of 5.5 meters. The period of field measurements encompassed two summer wet seasons; one was drier than normal and one was wetter than normal.

Water-balance components were measured, estimated, or computed as the residual in mass-balance computations. The water-balance components precipitation, evapotranspiration, and the rate of soil-water storage were measured or estimated using independent techniques. A layer of clay starting at a depth of 5.5 meters was assumed to limit vertical flow at that depth to negligible amounts. The equation for the water balance was arranged to compute water yield as the residual. Water yield was interpreted as being the sum of (1) the difference between surface-water inflow and outflow, (2) the difference between ground-water inflow and outflow, and (3) errors in the other water-balance components.

Alternative techniques were used to measure precipitation and evapotranspiration in order to assess the reliability of results. Precipitation was measured using tipping-bucket and accumulating rain gages. Precipitation recorded using the two gages agreed to within 1 percent. Evapotranspiration was estimated using the micrometeorological techniques energy-balance Bowen ratio (EBBR), energy-balance wind and scalar profile (EBWSP), and eddy correlation. Because reliable measurements of vapor-pressure gradients could not be routinely made at night and during early morning periods, and because numerical results from the EBBR technique are inherently unstable during early morning and evening periods, results from that technique were augmented using the EBWSP technique to produce continuous 24-hour records of evapotranspiration. Eddy-correlation measurements were made intermittently for 24-hour periods during the study. Daily evapotranspiration, computed using the combined EBBR-EBWSP approach, was significantly correlated with daily evapotranspiration estimated using eddy correlation ($r^2 = 0.89$). The slope of the relation between the two estimates was not significantly different from 1 and the intercept was not significantly different from 0.

Rate of soil-water storage was computed using a time series of replicated measurements of soil-water content. Volumetric soil-water content in the uppermost 0.15 meter of soil was measured using core samples. Volumetric soil-water content between depths of 0.15 and 1.7 meters was measured using a neutron moisture gage. Depth to the water table was never more than 1.7 meters during the study, and changes in water content between that depth and a depth of 5.5 meters were assumed to be negligible.

Precipitation during the 498 days of field measurements was 2,245 millimeters, which made it the largest component in the water balance. Evapotranspiration, the second largest component, was 1,419 millimeters. Water yield was 808 millimeters and the change in soil-water storage was 19 millimeters. When the water-balance was integrated annually to include the drier of the two wet seasons, precipitation was 1,019 millimeters, evapotranspiration was 1,000 millimeters, water yield was 215 millimeters, and the change in soil-water storage was -197 millimeters. When the water balance was integrated annually to include the wetter of the two wet seasons, precipitation was 1,561 millimeters, evapotranspiration was 981 millimeters, water yield was 540 millimeters, and the change in soil-water storage was 41 millimeters.

INTRODUCTION

Quantification of the major components of the hydrologic balance is essential when planning for the development and management of wildland ecosystems for water supply and for preservation of these systems in their natural state. The potential of an area for supplying a given amount of water on a continuous basis for domestic, agricultural, municipal, and industrial uses can best be established when the water balance of the area is examined during a sufficient period of time. In areas with pronounced wet and dry seasons, such as west-central Florida, the water-supply potential of surface-water systems and shallow ground-water systems changes greatly during the year, and knowledge of seasonal water-balance fluctuations can be used in estimating minimum reservoir capacity.

Development of wildland ecosystems in west-central Florida for water supply can affect the ecological integrity of these systems. Composition and structure of vegetative communities in low-lying areas are closely linked to availability of soil water throughout the year. If water is removed in substantial quantities, the composition and structure of wildland communities could be altered. Description of site water balances in one or more of these communities prior to development can be used as baseline information with which to interpret and describe effects of water-supply development.

Basinwide investigations have been made to quantify monthly and annual water balances of agricultural, wildland, and mixed agricultural and wildland basins in central and south Florida (Jones and others, 1984; Knisel and others, 1985). Results from the basinwide studies are useful for describing area average water-balance components; however, land-use types and soil and vegetation types are rarely constant, and the effects of individual soil or vegetation types on water-balance components, such as evapotranspiration, are difficult to determine with a basinwide approach.

Two other difficulties encountered in using mass-balance methods for describing basinwide water balances in central and south Florida are the spatial variability of precipitation and accurate determination of basin areas. A large fraction of the annual precipitation typically falls from convective cells that develop in the atmosphere during the wet season. The limited size of the cells can result in considerable spatial variation in precipitation over basins, which makes the task of determining basin precipitation inputs difficult, particularly for periods of a year or less (Capece and others, 1986). Additionally, drainage divides for undeveloped and undiked basins are difficult to determine accurately in the flat landscape of central and south Florida, and errors in determining basin area can introduce mathematical errors in the computation of water-balance components.

Purpose and Scope

This report presents some of the results from a 4-year study designed to examine the near-surface water balance of a site occupied by a common type of native vegetation in west-central Florida. The objectives of the study were to describe the site water balance on seasonal and annual timeframes and to develop, test, and implement a physically based model to simulate the unsaturated zone water balance. This report addresses the objective of describing the site water balance on seasonal and annual timeframes. The instruments and methods used to estimate the water-balance components of precipitation, evapotranspiration, changes in soil-water storage, and the differences between surface-water and ground-water inflows and outflows from the study area are described. This report also describes seasonal fluctuations of water-balance

components for June 4, 1991, to October 13, 1992, presents a sensitivity analysis for the water-balance computations, and interprets the results in terms of fundamental hydrologic processes and in the context of previous hydrologic studies.

Description of Study Area

The study was made on the T. Mabry Carlton, Jr., Memorial Reserve (Carlton Reserve) near State Road 72 in Sarasota County on the west coast of Florida (fig. 1). The Carlton Reserve lies on a sloping plain that ranges in altitude from 10 to 30 m above sea level. The plain is traversed by sloughs and the Myakka River that drain to the Gulf of Mexico. The land is flat. Slope gradients are generally less than 1 percent.

The humid, subtropical climate of west-central Florida reflects the latitude and proximity of this area to the Gulf of Mexico, Caribbean Sea, Atlantic Ocean, and the land mass of North America. The latitude of west-central Florida, which ranges from about 27°15′ to 29 °N latitude (fig. 1), establishes seasonal patterns of day length and effectively fixes the upper limit of clear-sky solar radiation that is received at the land surface. Smajstrla and others (1989) averaged daily solar radiation by month for Tampa, Fla. The annual average of daily solar radiation is about 17 $MJ/m^2 \cdot d$. The minimum monthly average of daily solar radiation is about 10 $MJ/m^2 \cdot d$ and occurs in December. The maximum monthly average of daily solar radiation is about 22 $MJ/m^2 \cdot d$ and occurs in May.

The influence of warm, moist air from the Caribbean Sea and the Gulf of Mexico, combined with intense solar heating, typically results in warm, wet summers in west-central Florida. The moist maritime air is driven over peninsular Florida by prevailing winds from the southeast and by sea breezes caused by temperature differences between the land and sea surfaces. Intense solar heating of the land surface often warms near-surface air temperature to more than 30°C during summer afternoons and can result in strong convective storms that can yield large amounts of rainfall in local areas. The wet season extends from June through September, and 60 to 70 percent of the annual rainfall occurs during these months. July and August were the warmest months in Tampa from 1951 to 1980, with a mean daily temperature of 28°C (National Oceanic and Atmospheric Administration, 1982).

Summer and early autumn are the seasons for hurricanes and tropical storms in Florida. In addition to high winds, these storms can deliver intense and widespread rainfall. The storms do not occur every year. The statistical return interval for hurricanes along the Gulf coast of west-central Florida is 12 to 17 years (Chen and Gerber, 1990). Less severe tropical disturbances occur more frequently than do hurricanes and can deliver substantial amounts of rainfall. Nonetheless, hurricanes and other tropical disturbances inflate the long-term rainfall statistics. During a year in which rainfall from tropical disturbances is small, rainfall amounts are likely to be less than the long-term average. Thus, droughts are common in west-central Florida in part because the occurrence of tropical storms is sporadic.

During late autumn and winter, the maritime influence of the Caribbean Sea and Gulf of Mexico alternates with weather systems from the land mass of North America to yield weather patterns in west-central Florida that can vary strikingly from day to day. In the absence of weather systems from the north, warm, moist air usually flows over west-central Florida from the south and southeast. Radiative heating of the land surface is less intense during late autumn and winter than during the summer, and convective storms are less frequent. Cold fronts occasionally sweep through Florida from the north during autumn and winter and sometimes deliver significant quantities of rainfall. In addition, air behind the front may be drier and tens of degrees Celsius cooler than the air ahead of the front. January was the coldest month at Tampa for 1951 to 1980; mean daily temperature was 15°C (National Oceanic and Atmospheric Administration, 1982).

Cold fronts become infrequent during spring, and prevailing winds from the south and southeast return to bring warm air to west-central Florida. However, the air can be dry during spring because of persistent high pressure over the eastern Atlantic Ocean. As a result, convective storms develop infrequently and the months of April and May are usually dry. Surface heating by solar radiation can drive temperatures higher than 30°C during the clear spring months. Effects of drought are most obvious during late spring. The warm, dry air and intense solar radiation combine to produce strong evaporative demand. If rainfall during the previous wet season and winter have been below normal, soil moisture deficits can become acute.

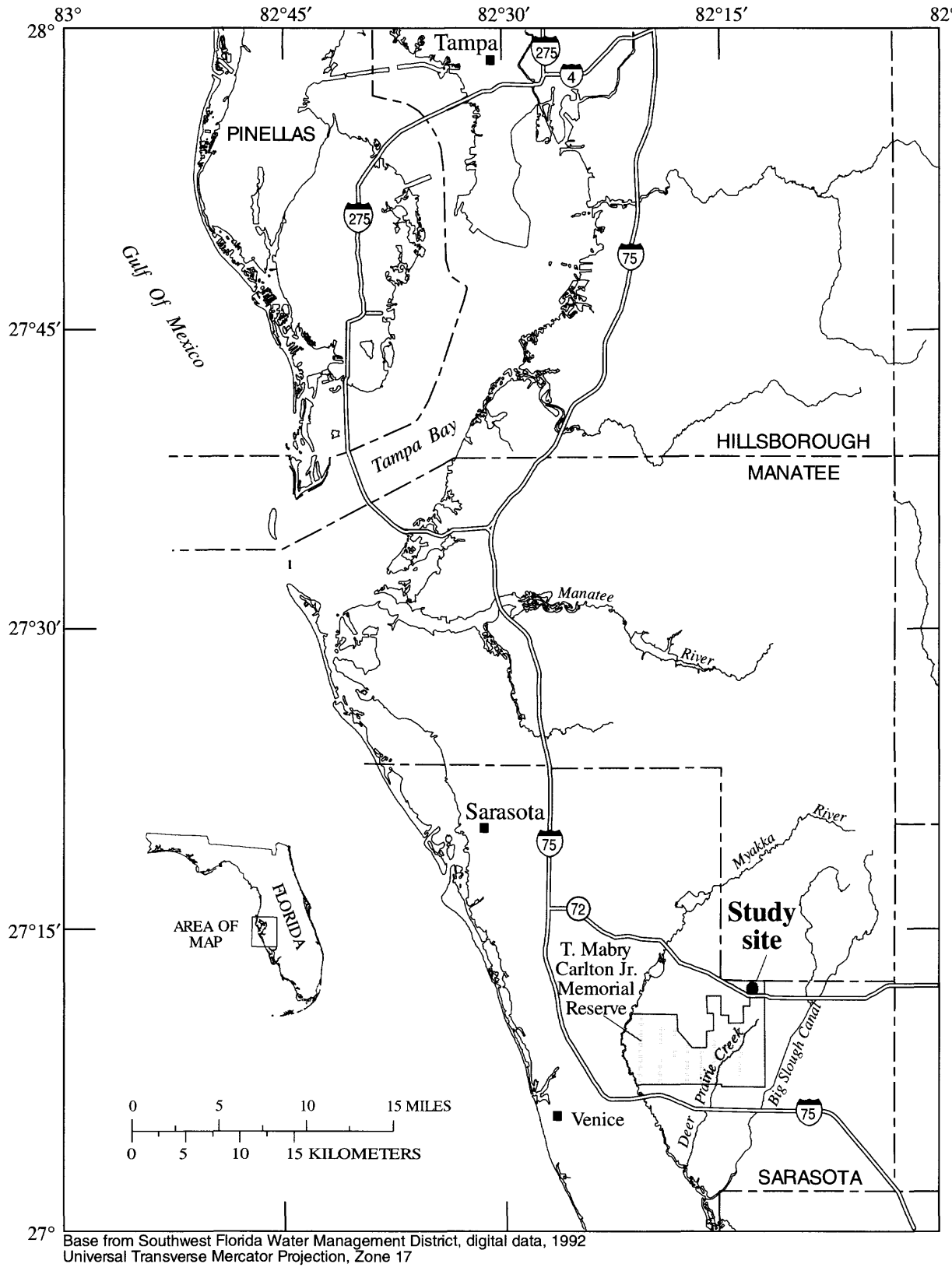

Figure 1. Location of study area and study site on the T. Mabry Carlton, Jr., Memorial Reserve, Sarasota County, west-central Florida.

Vegetation and Soils

The study site was within a vegetation type that can be classified either as dry prairie (Jeffrey Lincer, Sarasota County, written commun., 1990) or scrubby flatwood (Abrahamson and Hartnett, 1991). For descriptive purposes, the vegetation type will be referred to as dry prairie in this report. The site was treeless and the dominant species were saw palmetto (*Serinoa repens*) and wax myrtle (*Myrica cerifera*). Total vegetative cover appeared to be greater than 90 percent, and saw palmetto coverage was about 60 percent. Average canopy height was about 0.7 m. Other species represented at the site included the shrubs dwarf blueberry (*Vaccinium myrsinites*), running oak (*Quercus pumila*), and gallberry (*Ilex glabra*), as well as the grasses wiregrass (*Aristida spp.*) and beard grass (*Andropogon spp.*).

Dry prairie is a common vegetation type in west-central Florida in areas where the water table is rarely at the land surface. Except for the lack of trees, the dry prairie vegetation type is similar in many respects to the pine flatwood vegetation type. The treeless state of dry prairie sites probably results from historically short return intervals of wildfire. Species such as saw palmetto are adapted to fire disturbance; the plant has a massive root system and sprouts prodigiously after fire.

A recent soil classification map (Hyde and others, 1991) indicates that the soil at the study site is in either the EauGallie series (sandy, siliceous, hyperthermic Alfic Haplaquods) or the Myakka series (sandy, siliceous, hyperthermic Aeric Haplaquods). The distinction between these two series is slight, and diagnostic information collected during this study was not sufficient to classify the soils with certainty. Soils in both series are ground-water Spodisols that are common to the coastal plain of the southeastern United States (Hyde and others, 1991). Spodisols are characterized by extensive elluviation of organic matter, iron oxides, and clay from upper soil horizons to a soil horizon lower in the soil profile. Soils of the EauGallie and Myakka series are poorly drained, fine-sandy, mineral soils that occur on nearly level terrain. The water table ranges seasonally from the soil surface to depths of more than 1 m. The mineral fraction is dominated by fine quartz sand. Silt mass fraction is less than 10 percent and clay mass fraction is less than 5 percent. The developed soil profile at the site extends to a depth of about 2.5 m.

The developed soil profile is underlain by sands and sand-clay mixes to a depth of about 5.5 m. The soil and underlying sediments compose the uppermost parts of the surficial aquifer, and the total thickness of that aquifer is about 20 m (Duerr and Wolansky, 1986). Although the term "soil" is usually reserved for near-surface materials that are the result of recognized soil-forming processes, many of the physical and chemical properties of deeper, unconsolidated materials are similar to those of soils. For this reason, and for the sake of simplicity, the term "soil" is used in this report to refer to the developed soil profile and to the underlying sands and clays.

DESCRIPTION OF NEAR-SURFACE WATER-BALANCE COMPONENTS

The instantaneous water balance of a saturated or partially saturated soil column of unit horizontal area can be described by the equation

$$P = E + \int_0^{D_0} \frac{\partial \theta}{\partial t} dz - q_{ri} + q_{ro} - q_{si} + q_{so} + qd \,, \quad (1)$$

where

P is precipitation, in millimeters per day;

E is evapotranspiration, in millimeters per day;

$\int_0^{D_0} \frac{\partial \theta}{\partial t} dz$ is the rate of soil-water storage, in millimeters per day; where D_0 is vertical thickness of the soil column, in millimeters; $\partial\theta/\partial t$ is rate of change of volumetric soil-water content with respect to time, per day; and z is depth, in millimeters;

q_{ri}, q_{ro} are the lateral flows of surface-water into the area and out of the area, respectively, in millimeters per day;

q_{si}, q_{so} are the lateral, flows of ground water into the column and out of the column, respectively, in millimeters per day; and

q_d is vertical water flow at depth $z = D_0$, in millimeters per day.

Equation 1 can be integrated to describe the water balance for any time period if the variation in time of each water-balance component used for the integration is known.

Although the water-balance equation is defined for a unit area of land surface, the depth over which the equation is to be applied needs to be specified. The control volume for water-balance calculations is fully defined when the depth to the lower boundary is specified. In this study, a layer of clay, the upper surface of which was present at a depth of about 5.5 m, was used as the lower boundary for the water-balance calculations. The clay layer was selected because it was below the water table during the study, which meant that changes in soil-water storage below that depth were small and did not have to be considered, and because it constituted a nearly impermeable hydrologic barrier, which simplified the evaluation of vertical water flow.

The water-balance equation can be arranged to compute a single component or a sum of components as a residual. In this study, the components precipitation, evapotranspiration, rate of soil-water storage, and vertical water flow were computed from field measurements. Equation 1 was arranged to solve for the difference between lateral inflows and outflows ($q_{ro} - q_{ri} + q_{so} - q_{si}$). This quantity can be termed "water yield" because the difference between horizontal inflow and outflow is the amount of water per unit of land-surface area per unit time that is discharged from the study area.

Field and laboratory measurements were used to determine or estimate the water-balance components—evapotranspiration, the rate of soil-water storage, precipitation, and vertical water flow. Evapotranspiration was estimated using three micrometeorological techniques. The rate of soil-water storage was estimated by a time series of replicated measurements of soil-water content. Precipitation was measured using a tipping-bucket rain gage and an accumulating rain gage. Vertical water flow at the bottom of the control volume was computed with a flux equation for saturated flow using estimates of soil hydraulic conductivity and a time series of measurements of vertical gradients in hydraulic head. Water-balance components were monitored at the field site from June 4, 1991, to October 13, 1992.

Techniques and Instrumentation Used to Estimate Evapotranspiration and Potential Evapotranspiration

Three different micrometeorological techniques were used to estimate evapotranspiration: the energy-balance Bowen ratio (EBBR), the energy-balance wind and scalar profile (EBWSP), and the eddy-correlation techniques. Multiple techniques were used because, in the absence of independent knowledge of actual evapotranspiration, comparison of results from different techniques provides a basis for assessing the reliability of the results. If results from two or more independent and theoretically sound techniques are similar, it is reasonable to expect that they are similar because each closely approximates actual evapotranspiration. In addition, the techniques used in this study rely on different ensembles of micrometeorological measurements, and reliability of the individual sensors can vary depending on environmental conditions. Also, outright instrument failure is a persistent threat to the integrity of data sets collected in the field. The use of multiple techniques permits investigators to take advantage of the strengths of each to produce a more reliable record of evapotranspiration.

The micrometeorological techniques discussed above rely on measurements that are typically made within a few meters to a few tens of meters above a surface and within the surface sublayer of the atmospheric boundary layer. The surface may be bare or vegetated soil, or it may be water. Under steady conditions and in the absence of horizontal gradients, vertical fluxes of heat and water vapor within the fully turbulent surface sublayer are not appreciably different from fluxes at the surface (Brutsaert, 1982, p. 54), and surface fluxes can be estimated by determining vertical fluxes within the surface sublayer.

The absence of horizontal gradients in vertical fluxes of momentum, heat, and water vapor is an important condition for the one-dimensional EBBR, EBWSP, and eddy-correlation techniques. When the mean horizontal wind has passed over a uniform surface for a sufficient distance, a layer of air develops near the surface in which horizontal gradients in vertical fluxes of momentum, heat, and water-vapor are small fractions of the vertical fluxes themselves. This layer of air can be said to have equilibrated with the surface because windspeed, temperature, and water-vapor profiles reflect surface roughness and temperature, and moisture conditions

of the surface. Energy-balance Bowen ratio, EBWSP, and eddy-correlation measurements should be made within the equilibrated layer of air.

As the wind passes from one type of surface to another, such as from a prairie to a marsh, horizontal gradients in vertical fluxes of momentum, heat, and water vapor may develop across the leading edge of the downwind surface because the airstream begins to exchange momentum, heat, and water vapor with the different downwind surface. Downwind from the surface change, the layer of equilibrated air begins to rebuild from the surface. The thickness of this layer increases with distance downwind.

Fetch-instrument height guidelines are used by practitioners to determine where instruments can be placed to ensure that they will operate within the equilibrated layer of air. Under these guidelines, measurements should be taken at a height above a surface not greater than a specified fraction of the distance downwind from a surface change. This fraction has been reported variously as 0.01 (Campbell, 1977, p. 40), 0.01 to 0.003 (Tanner, 1988), and 0.05 (Heilmman and Brittin, 1989) depending on such factors as the abruptness of the surface roughness change and atmospheric stability.

Potential evapotranspiration techniques can be used to obtain realistic estimates of evapotranspiration under some field conditions, and data and instrumentation requirements for them are typically much less stringent than are requirements for techniques such as EBBR, EBWSP, and eddy correlation. An analysis using the concept of potential evapotranspiration was applied in this study and results were compared to evapotranspiration determined using eddy correlation to evaluate the suitability of that potential evapotranspiration technique for estimating actual evapotranspiration.

Energy-Balance Bowen Ratio

The EBBR technique (Bowen, 1926) has been used extensively to estimate evapotranspiration in different terrestrial environments. The EBBR technique is based on an observation that evapotranspiration is a form of energy exchange between a surface and the atmosphere. Because of this, water and energy exchange are coupled when the surface is partially wet. This coupling can be expressed in terms of the surface energy balance. By omitting energy storage due to photosynthesis and heat storage in a plant canopy, an equation for the energy balance of a surface can be written

$$R_n - G - H - \lambda E = 0 , \qquad (2)$$

where

R_n is net radiation for the surface, in watts per square meter;

G is subsurface heat flux, in watts per square meter;

H is sensible heat flux, in watts per square meter; and

λE is latent heat flux, in watts per square meter, where λ is heat of vaporization for water (2,430 J/g at 30°C); and E is evapotranspiration, in grams per square meter per second.

Net radiation is the sum of all incoming radiation streams minus the sum of outgoing radiation streams. Incoming direct and diffuse solar radiation dominate net radiation during the day, and outgoing thermal radiation is typically the largest component of net radiation at night. Subsurface heat flux is the exchange of heat between the surface and the underlying medium. For terrestrial environments, the medium is usually soil. The quantity (R_n -G) may be referred to as "available energy." Exchange of sensible and latent heat is dominated by turbulent transport, and to a large extent the exchange is driven by available energy. Photosynthesis accounts for only a few percent of R_n at most, and Bidlake and others (1993) determined that heat storage in the plant canopy was unimportant for the purpose of estimating daily evapotranspiration from dry prairie vegetation. The sign convention for flux direction is: R_n is positive when the net radiation flux is directed toward the surface, G is positive when the subsurface heat flux is directed downward, and H and λE are positive when the fluxes are directed away from the surface.

The ratio of sensible to latent heat flux, the Bowen ratio, is given by

$$\beta = \frac{H}{\lambda E} = \frac{-K_h \rho_a C_p \left(\Delta\theta/\Delta z\right)}{-\lambda K_v \rho_a \varepsilon/p \left(\Delta e/\Delta z\right)} , \qquad (3)$$

where

β is the Bowen ratio, dimensionless;

K_h is eddy diffusivity for heat, in square meters per second;

K_v is eddy diffusivity for water vapor, in square meters per second;

ρ_a is density of air, in grams per cubic meter;

C_p is specific heat of air at constant pressure, in joules per gram per kelvin;

$\Delta\theta$ is potential temperature difference over a vertical interval above the surface, in kelvins;

Δz is length of the vertical interval, in meters;

Δe is vapor-pressure difference over the vertical interval, in kilopascals;

ε is the ratio of molecular mass of water to that of dry air, dimensionless;

p is total atmospheric pressure, in kilopascals; and other terms are as previously defined.

An important premise of the EBBR technique is that eddy diffusivities for heat and water-vapor transport are approximately equal. Then, if air temperature and vapor-pressure measurements are made over the same vertical interval, a close approximation to equation 2 for work within a few meters of a surface is

$$\beta \approx \gamma \frac{\Delta T}{\Delta e}, \qquad (4)$$

where

ΔT is air-temperature difference over a vertical interval above the surface, in degrees Celsius;

γ is the psychrometer coefficient, in kilopascals per degree Celsius; and the psychrometer coefficient is computed from $\gamma = pC_p/\lambda\varepsilon$, where terms are as previously defined.

If R_n, G, and β are known, equation 2 may be solved for λE

$$\lambda E = \frac{R_n - G}{1 + \beta}. \qquad (5)$$

Net radiation measurements.—Net radiation was sensed using a net radiometer (Gates, 1962, p. 81). The net radiometer (Model Q-5, Radiation and Energy Balance Systems, Inc.) had upward- and downward-facing sensing surfaces that were the outer surfaces of a 62-junction thermopile. In operation, greater radiation heating of one surface with respect to the other resulted in a temperature difference between the two sides, and this was sensed by the voltage output from the thermopile. The voltage output was related to the difference in incident radiation between the two surfaces by a calibration factor. The sensing surfaces were protected from convective heat exchange and the weather by hemispherical windshields made from clear polyethylene (thickness approximately 0.25 mm). Two net radiometers were available, which permitted them to be exchanged when calibration or repair was needed. Radiometers were mounted at a height of 2.3 m. Net radiation was measured every 10 seconds and was averaged over 20-minute periods.

Each radiometer was returned to the manufacturer for windshield replacement and calibration twice during the 16-month data-collection period. Results from the calibrations indicated that the maximum drift in instrument calibration was less than 2 percent. Windshields became scratched after repeated cleaning, and they also became slightly discolored, presumably due to exposure to solar radiation. The windshields were replaced after about 3 months of service. To investigate possible errors caused by weathered windshields, calibration of one radiometer was checked before and after windshield replacement. No difference in calibration factors was observed. Finally, measured net radiation was adjusted on the basis of comparisons between the Model Q-5 and a more recent model (Leo Fritschen, University of Washington, written commun., 1990). The adjustments were:

$$R_n = 0.986 + 0.947R_n^* \quad \text{for } R_n^* > 0$$

$$R_n = -0.381 + 0.992R_n^* \quad \text{for } R_n^* < 0,$$

where R_n^* is unadjusted net radiation (measured using the Model Q-5 net radiometer), in watts per square meter.

Estimation of subsurface heat flux.—Subsurface heat flux was estimated using the equation

$$G = G_z + z\left(C_s\rho_b + \rho_w C_w \theta\right)\frac{\Delta T_s}{\Delta t}, \qquad (6)$$

where

G_z is average measured heat flux at depth z in the soil, in watts per square meter;

ΔT_s is the change in average soil temperature to depth z during an averaging period, in degrees Celsius;

C_s is specific heat of soil particles, in joules per gram per degree Celsius;

ρ_w is density of water, in grams per cubic meter;

ρ_b is bulk density of the soil, in grams per cubic meter;

C_w is specific heat of water, in joules per gram per degree Celsius;

θ is volumetric soil-water content, dimensionless;

z is soil depth, in meters; and

Δt is duration of the averaging period, in seconds.

Data collected using soil heat flux plates and soil temperature sensors were used with equation 6 to compute soil heat flux at the soil surface. The heat flux plates (Model HFT-1, Radiation and Energy Balance Systems, Inc.) were used to sample sensible heat flux in soil (G_z) at a depth of 10 cm. The plates were buried parallel to the soil surface so as to sense vertical heat flux. Total heat flux in moist, unsaturated soil consists of both sensible and latent heat fluxes. The plates obstruct latent heat transport, which may account for 15 percent of the total heat flux (Campbell, 1985, p. 34), and thus result in measurement error. To reduce this measurement error, the suggestion of Tanner (1960) was followed, and the plates were buried at a depth of 10 cm.

The second term on the right side of equation 6 is included to account for the rate of soil heat storage above the heat flux measurement. The rate of heat storage was estimated by calorimetry. Soil temperature was measured using averaging temperature probes (Model TCAV, Campbell Scientific, Inc.), which consisted of four chromel-constantan thermocouples. The thermocouples were spaced vertically at approximately even intervals to a depth of 10 cm in an attempt to make thermocouple output represent average temperature in the upper 10 cm. Data for the remaining parameters in equation 6 were supplied using handbook values and additional field sampling. For the quartz-rich mineral soils encountered in this study, C_s was estimated to be 0.8 J/g•°C, and an accepted value for C_w is 4.18 J/g•°C (Campbell, 1985, p. 32). A drive-core sampler was used to collect samples of known volume for determination of ρ_b and θ. Soil samples were collected periodically from three locations, weighed, dried for a minimum of 24 hours at 105°C, and weighed again to determine ρ_b and θ. Soil-water content in the uppermost 10 cm varied during the study, and when θ was not sampled, it was estimated from water-table depth, which was monitored continuously, using the relation

$$\theta = 0.442 - 0.198D$$

$$S_{y \bullet x} = 0.031 \quad n=22,$$

where

D is depth of the water table, in meters;

$S_{y \bullet x}$ is standard error of estimate, dimensionless; and

n is sample size, dimensionless.

The above relation oversimplified the water balance of the top 10 cm of soil; however, the EBBR calculation for latent heat flux (λE) is not sensitive to soil-moisture content over the ranges of soil moisture and soil temperature difference encountered in this study. The above statistical relation probably was adequate for the particular site for which it was developed.

Subsurface heat flux typically varies horizontally because of partial shading of the soil surface, topographic effects, or other factors that affect the surface energy balance. The heat flux plates and temperature probes described above provide only point measurements; therefore, replicate heat flux measurements were made in an attempt to determine the average heat flux and the spatial variability of heat flux. The number of heat flux plates used for those measurements ranged from three to six during the study, and the number of soil temperature probes ranged from three to five. Soil heat flux was measured every 10 or 60 seconds and averaged for 20-minute periods. Soil temperature was measured at the beginning and end of each 20-minute period.

Bowen ratio determination.—The air temperature and vapor-pressure differences needed to compute the Bowen ratio (eq. 4) are difficult to measure because temperature and vapor-pressure differences over a vertical interval of 1 to 2 m above a vegetated surface can be small. Daytime temperature and vapor-pressure differences over a densely vegetated surface are typically a few tenths of a degree and a few hundredths of a kilopascal, respectively. The magnitudes of the differences at night are smaller. The differences commonly are near the resolution limits of available instrumentation. In addition, measurement errors attributable to the field environment, such as radiative heating of temperature sensors, can easily lead to erroneous measurements of temperature and vapor-pressure differences.

The Bowen ratio system that was described by Tanner and others (1987) was used in this study. That system had the potential for unattended operation because vapor-pressure determination was accomplished with a dewpoint hygrometer, thus

avoiding the difficulties caused by drying or contaminated wicks that can occur with psychrometric instruments (Duell, 1990). A pump alternately drew air from upper and lower sampling ports at 2-minute intervals during a 20-minute averaging period, and the air was introduced into the hygrometer (Model Dew-10, General Eastern, Inc.) for determination of the dewpoint. The vapor pressure of each air stream was determined from an equation for saturation vapor pressure evaluated at the dewpoint temperature (Lowe, 1977). Air temperature differences over a fixed vertical interval were sensed with a pair of chromel-constantan thermocouples. The thermocouples were fixed at the end of horizontal 1.5-m support arms, and the air intakes were fixed about half way along the arms. System measurement and control functions were performed by a data logger (Model 21X, Campbell Scientific, Inc.). The manufacturer indicates that the system resolution for vapor pressure and the temperature difference are better than 0.01 kPa and 0.006°C, respectively. The lower thermocouple and air intake were 1.6 m above land surface, and the upper thermocouple and air intake were 2.6 m above land surface. EBBR measurements were made continuously from June 4, 1991, until October 13, 1992, except during periods when the Bowen ratio system was shut down for repairs or maintenance.

The thermocouples were not shielded from radiation and they were not ventilated; therefore, it was critical that other aspects of their design were optimized for accurate measurement. This was accomplished by constructing the thermocouples using a small-diameter wire to reduce the role of radiation relative to convective heat exchange in the total sensor energy balance. Small thermocouple wires are easily broken by flying insects, raindrops, and airborne debris, so the wires had to be large enough to withstand most common hazards. The manufacturer recommended thermocouple wire that is 76 µm in diameter for use in field environments, and this generally was durable enough for the hazards that were encountered in this study.

Another aspect of sensor design relied on the fact that it is primarily the difference in air temperature, not absolute air temperature, that must be accurately determined if the Bowen ratio is to be determined reliably. If upper and lower thermocouples absorb the same radiation load, the error in determining the temperature difference would be much smaller than the error in determining absolute temperature. If both thermocouples are to be heated equally, it is critical that they exhibit similar geometries with respect to solar beam and diffuse radiation.

Measured temperature differences determined using two presumably identical sets of thermocouples were compared at the field site to examine potential effects of radiation heating on the variability of the temperature difference measurement. Comparisons were made using 76- and 25-µm diameter thermocouple wire. Results from the comparisons are discussed in the section **"Evapotranspiration Error."**

The sensitivity of the dewpoint hygrometer was checked using an Assman wet-bulb and dry-bulb psychrometer. The comparisons were performed using a stirred environmental chamber. The wet-bulb and dry-bulb psychrometer was placed in the chamber for measurement of the wet-bulb and dry-bulb temperatures. Air from the chamber was pumped to the external dewpoint hygrometer, where the dewpoint was measured, and then back into the chamber. Vapor pressure of the chamber was varied from 0.8 to 3.0 kPa by controlling the flow rate of desiccated air into the chamber. A small vent in the chamber was presumed to maintain total pressure inside the chamber approximately equal to ambient atmospheric pressure. Dewpoint temperature and wet-bulb and dry-bulb temperatures were recorded when the dewpoint hygrometer indicated that vapor pressure within the chamber had reached steady state. Air temperature in the chamber, which was not controlled, ranged from 25.8 to 30.1°C. The response of vapor pressure computed using the dewpoint hygrometer matched the response of vapor pressure computed using the psychrometer to within 2 percent (fig. 2).

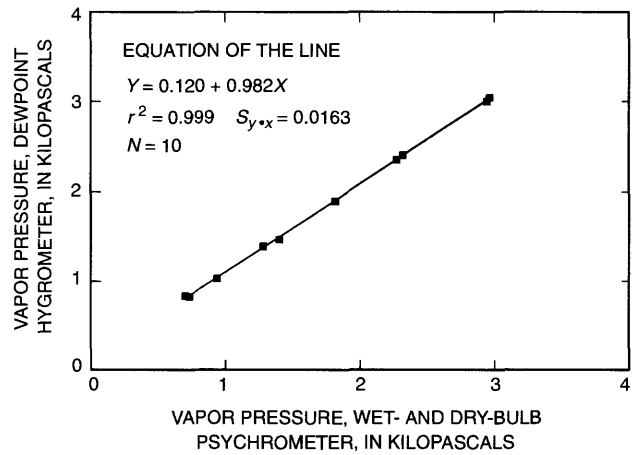

Figure 2. Relation between vapor pressure determined using a dewpoint hygrometer and vapor pressure determined using a wet-bulb and dry-bulb psychrometer.

Operation and design of the Bowen ratio system were modified in an attempt to minimize condensation in the vapor-pressure sampling system. Previous experience indicated that moisture commonly condensed in the system tubing when air was drawn in at night and in the early morning. During some days, the moisture would persist until midday or later, thereby invalidating the EBBR calculation for latent heat flux for a significant part of a day. The modifications were (1) vapor-pressure sampling was discontinued at night; (2) the air intakes were shielded using ducts constructed from aluminum sheeting to keep the air intake filters dry during rainfall and dewfall; and (3) heaters were installed to raise the temperature of air intakes, tubing, and other surfaces that contacted the air sample above the dewpoint temperature. The ducts were heated with ceramic power resistors to dry them out each morning before air sampling began. Air intake lines were heated using heat tape. The enclosure housing the switching valves, dewpoint hygrometer, and air-sample mixing bottles was heated using power resistors. The heaters were energized about an hour before air sampling began each morning and heating continued for 3 to 4 hours.

Despite the above steps, condensation continued to affect vapor-pressure sampling during the first hour or two, and occasionally more, of most mornings. The problem persisted primarily due to a lack of electrical power for the heaters, which came from two 18-watt solar panels connected to a 12-volt lead-acid storage battery. The small amount of power limited the maximum heating wattage and the number of hours of heating each day. The arguments presented by Ohmura (1982) were used to detect erroneous Bowen ratio data, and those data were excluded from EBBR flux computations.

Energy-Balance Wind and Scalar Profile

In the EBWSP technique (Stricker and Brutsaert, 1978), net radiation (R_n), subsurface heat flux (G), and sensible heat flux (H) are measured or estimated and the equation for the surface energy balance is solved for latent heat flux (λE)

$$\lambda E = R_n - G - H. \tag{7}$$

Methods for determining net radiation and subsurface heat flux were discussed previously. Additional work needed to use the EBWSP technique involves estimation of sensible heat flux.

A flux-profile equation for sensible heat flux (H) that is applicable under steady conditions and near an extensive homogeneous surface is (Stricker and Brutsaert, 1978)

$$H = \frac{u^* k \rho_a C_p \Delta T}{\ln\left\{\frac{(z_2-d)}{(z_1-d)}\right\} - \Psi_h\left\{\frac{(z_2-d)}{L}\right\} + \Psi_h\left\{\frac{(z_1-d)}{L}\right\}}, \tag{8}$$

where

u^* is friction velocity, in meters per second;
k is the von Karman constant (approximately 0.4), dimensionless;
z is height, in meters;
d is zero-plane displacement height, in meters;
L is the Obukhov stability length, in meters;
Ψ_h is the operator for the diabatic profile correction function for heat, dimensionless;
1, 2 indicate measurements made at lower and upper heights above the surface, respectively; and
other terms are as previously defined.

If horizontal windspeed is measured at some height z_w, in meters, friction velocity may be computed from

$$u^* = \frac{uk}{\ln\left\{\frac{(z_w-d)}{z_0}\right\} - \Psi_m\left\{\frac{(z_w-d)}{L}\right\}}, \tag{9}$$

where

u^* is horizontal wind speed, in meters per second;
z_0 is roughness length for momentum, in meters;
Ψ_m is the operator for the diabatic profile correction function for momentum, dimensionless; and
other terms are as previously defined.

The diabatic profile correction functions are included in the analysis to account for the effects of nonneutral atmospheric stability on turbulent transport. Diurnal heating and cooling of air near the surface or evaporation of water into that air changes the density of the air. When air near the

surface becomes less dense than air aloft, it becomes buoyant, which enhances turbulent transport of momentum, heat, and moisture. The atmosphere is termed unstable when air near the surface becomes buoyant. If air near the surface becomes less buoyant, the intensity of turbulent transport is dampened, and the atmosphere is termed stable. A neutral atmosphere exists when buoyancy is neutral.

Atmospheric stability can be characterized using the Obukhov stability length (Brutsaert, 1982), which is given by

$$L = \frac{-u^{*3}\rho_a}{kg\,[\,(H/T_kC_p) + 0.61E]}\,, \qquad (10)$$

where g is gravitational acceleration, approximately 9.8 m/s^2; T_k is air temperature, in kelvins; and other terms are as previously defined. The stability length is negative when the atmosphere is unstable and positive when the atmosphere is stable. The magnitude of L approaches infinity when neutral conditions exist.

The specific formulations of the profile correction functions are not universally established in the literature, particularly for stable conditions (Brutsaert, 1982, p. 71). Stricker and Brutsaert (1978) observed that stability corrections were important, but also that the sensible heat computations were not particularly sensitive to the selection of a given set of profile correction functions from the literature. The following profile correction functions were taken from Brutsaert (1982) and used in this study:

$$\Psi_m = \Psi_h = -5\frac{(z-d)}{L} \text{ for } L>0; \qquad (11a)$$

$$\Psi_m = 2\ln\left[\frac{(1+x)}{2}\right] + \ln\left[\frac{(1+x^2)}{2}\right] - 2\arctan(x) + \frac{\pi}{2} \text{ for } L<0; \qquad (11b)$$

and

$$\Psi_h = 2\ln\left[\frac{(1+x^2)}{2}\right] \text{ for } L<0, \qquad (11c)$$

where

$x = [1\text{-}16\,(z\text{-}d)\,/\,L]^{1/4}$, and

other terms are as previously defined.

Equation 8 cannot be solved for H and E explicitly but an iterative scheme can be used to solve for them. Once values for R_n, G, ΔT, u, z_1, z_2, z_w, z_0, and d were supplied, the following procedure was used to solve for sensible (H) and latent (λE) heat fluxes:

1. Set L equal to a large number (for example, 10,000), thus assuming a neutral atmosphere;
2. Evaluate diabatic profile correction functions (eqs. 11a, 11b, and 11c);
3. Compute u^* (eq. 9);
4. Compute H and E (eqs. 7 and 8);
5. Compute L (eq. 10); and
6. Repeat starting at step 2.

The iteration was continued until L changed by less than a specified amount or until a specified number of iterations had been performed, whichever came first. If the procedure did not converge to a single value for L, the computation for sensible heat flux was rejected for the time period under examination, and the EBWSP technique was not used to estimate latent heat flux.

Data for computing sensible heat flux were collected at the dry prairie site. The temperature difference (ΔT) was the difference measured for the EBBR calculation. Horizontal windspeed at a height of 2.6 m was measured continuously using a pulse-generating cup anemometer (Model 014A, Met-One, Inc.) and a data logger, or it was measured every 10 seconds using a direct-current generator cup anemometer (Model 12102, R.M. Young Co.) and a data logger. Horizontal windspeed was averaged every 20 minutes. The computed sensible heat flux is quite sensitive to the values for the surface roughness parameters z_0 and d (Stricker and Brutsaert, 1978). The estimation of those parameters is described below.

Eddy Correlation

General equations for turbulent transport may be simplified when applied to vertical atmospheric transport near an extensive homogeneous surface (Brutsaert, 1982, p. 190). In the absence of horizontal gradients, and by ignoring transport by molecular diffusion, equations for sensible and latent heat flux may be written

$$H = \rho_a C_p \overline{w'T'}\,; \qquad (12)$$

and

$$\lambda E = \lambda \overline{w'\rho_v'}\,, \qquad (13)$$

where

w is vertical windspeed, in meters per second;

T is air temperature, in degrees Celsius;

ρ_v is vapor density, in grams per cubic meter;

$'$ represents a momentary fluctuation from the mean;

$\overline{}$ represents a time average; and

other terms are as previously defined.

The eddy-correlation system described by Bidlake and others (1993) was used for eddy-correlation measurements in this study. Fluctuations in vertical wind speed and air temperature were sensed with a one-dimensional sonic anemometer equipped with a fine-wire thermocouple (Model CA-27, Campbell Scientific, Inc.). Operating principles and characteristics of that instrument are presented in Campbell and Unsworth (1979), Weeks and others (1987), and Tanner (1988). Fluctuations in vapor density were sensed with a krypton hygrometer (Model KH20, Campbell Scientific, Inc.). Operating principles and characteristics of that instrument are presented in Campbell and Tanner (1985), Tanner and others (1985), and Tanner (1988). A data logger was used to query each sensor at 10 *Hz* and to compute the covariances $\overline{w'T'}$ and $\overline{w'\rho_v'}$ every 20 minutes. The 20-minute covariances were computed as the average of four 5-minute covariances that were computed from

$$\overline{w'Y'} = \frac{\Sigma wY}{n} - \frac{\Sigma w \Sigma Y}{n^2},$$

where

Y is temperature, in degrees Celsius, or vapor density, in grams per cubic meter;

n is the number of samples in a 5-minute period; and other terms and symbols are as previously defined.

Latent heat flux was corrected for the effects of sensible heat flux (Webb and others, 1980) and hygrometer sensitivity to fluctuations in concentration of molecular oxygen (Tanner and Greene, 1989). The hygrometer was returned to the manufacturer for calibration in March 1992 and it was noted that the calibration factor had changed by less than 2 percent since a factory-calibration in December 1989.

Sensible and latent heat fluxes determined by eddy correlation were combined with measurements of net radiation and subsurface heat flux to evaluate energy-balance closure by the equation

$$C = \frac{H + \lambda E}{R_n - G}. \qquad (14)$$

Any value of C other than 1.0 indicates that the ensemble of energy-balance measurements is inconsistent and that either additional energy-balance terms need to be considered or that the existing terms are in error.

Eddy-correlation measurements were made about once a month from June 1991 to September 1992. Measurements were typically made for 24 hours or more, and sensible and latent heat fluxes were computed for each 20-minute period. The midpoint of the measurement paths of the sonic anemometer and the krypton hygrometer were set at a height of 2.1 m above land surface.

Estimation of Surface Roughness Parameters

Estimation of sensible heat flux by use of the flux-profile relation (eq. 8) requires that values be supplied for the zero-plane displacement height (d), in meters; and the surface roughness length (z_0), in meters. Stricker and Brutseart (1978) found that the sensible heat predicted using equation 8 varied strongly with d and particularly z_0 when air temperature gradients were determined close to a vegetated surface. If computed sensible heat flux is sensitive to d and z_0, an inverse method should be effective for estimating the parameters. The approach in this study was to simultaneously measure, vertical air temperature difference (ΔT), horizontal wind speed (u), sensible heat flux (H), and evapotranspiration (E) above the dry prairie vegetation. A nonlinear least squares procedure was then used to solve for d and z_0.

Instrumentation and measurements used to determine the input variables for the inverse procedure were discussed previously in this report. The cup anemometers were not reliable for determining mean horizontal windspeed when it approached instrument stall speeds, and data were included in the analysis only if the average wind speed was greater than 0.5 m/s. Also, the behaviors of the profile correction functions are not well understood for stable conditions (Brutsaert, 1982, p. 71); therefore, only data collected under unstable conditions ($H>0$) were used. Data from sixteen 24-hour periods, collected between June 1991 and September 1992, were pooled for the analysis. All variables were averaged and recorded at 20-minute intervals, and data from 452 such intervals were used.

The roughness parameters were estimated by minimizing the sum of the squared residuals for the function

$$H_{ec} - H_{ebwsp} = 0 , \quad (15)$$

where

H_{ec} is sensible heat flux for a 20-minute period measured using eddy correlation, in watts per square meter; and

H_{ebwsp} is sensible heat flux for a 20-minute period predicted using equation 8.

The value of H_{ebwsp} was computed by iteratively solving equations 8, 9, 10, and 11a through 11c as described in the presentation of the EBWSP method. The procedure of Marquardt (1963) was used to solve equation 8 for the parameters d and z_0. First, d was supplied as a constant and the procedure would be used to solve for z_0. Second, the value for z_0 was supplied as a constant and the procedure would be used to solve for d. Initial values of d and z_0 were computed from average canopy height as suggested by Campbell (1985). Iteration between solutions for d and z_0 was continued until the parameters were changed by less than 0.01 m. The output value for d was quite sensitive to the input value for z_0; however, the output value for z_0 was much less sensitive to the input value for d.

Linear-regression analysis indicated a strong relation between H_{ec} and H_{ebwsp} when effects of atmospheric stability were included (table 1). The relation was weaker, but still significant ($P<0.05$), when stability corrections were not used. The importance of accounting for atmospheric stability also is indicated by the intercept and slope parameters presented in table 1. In an ideal relation, the intercept would be 0 and the slope would be 1. The analysis that included a stability correction yielded a more nearly ideal relation.

Table 1. Roughness parameters d and z_0 and relation between sensible heat flux estimated using eddy correlation and sensible heat flux estimated using equation 8

[d, zero-plane displacement height, in meters; z_0, surface roughness length for momentum transport, in meters; a, intercept, in watts per quare meter; b, slope, dimensionless, for the relation: $H_{ec}=a+bH_{ebwsp}$, where H_{ec} is sensible heat flux estimated using eddy correlation, and H_{ebwsp} is sensible heat flux estimated using equation 8]

Stability correction?	d	z_0	a	b	n	r^2
Yes	0.72	0.12	[1]7.72	0.96	452	0.86
No	.73	.25	[1]22.54	[1].87	452	.71

[1]At the 1-percent probability level, intercept is significantly different from 0 or the slope is significantly different from 1.

The computed values for d and z_0 agreed closely with values estimated using measurements of canopy structure and empirical relations suggested by Campbell (1985). For dense plant canopies, Campbell recommends: $d = 0.77h_c$, where h_c is height of the plant canopy, in meters; and $z_0 = 0.13h_c$. Values for d and z_0 estimated from these relations and measurements of height of six individual palmetto made in April 1992 and again in November 1992 were 0.68 and 0.11, respectively. The plant canopy was dense and fairly uniform, and the empirical relations were probably applicable. The empirical relations indicate that the roughness parameters may be expected to change as a canopy grows in height. A single set of roughness parameters were used for the analysis presented here because canopy height changed little during the study. Palmetto, which was dominant at the site, is an extremely slow growing plant above ground. The repeated measurements of six individual plants indicated no significant height growth ($P>0.05$) even though the 7-month period between measurements encompassed the wet season when maximum growth would be anticipated.

Approaches for Estimating Daily Evapotranspiration

Daily evapotranspiration, in millimeters per day, was computed by first summing 20-minute latent heat flux for 24-hour periods to yield daily latent heat flux, in megajoules per square meter per day. Second, daily latent heat flux was multiplied by 0.411, which is the appropriate conversion factor if values for λ (2,430 J/g) and ρ_w (1.0 Mg/m^3) are assumed.

Two independent approaches were used to estimate evapotranspiration and daily latent heat flux. In the first approach, results from the EBBR and EBWSP techniques were combined. This combination approach was used because continuous 24-hour records could not be assembled using the EBBR technique alone. The EBBR technique could not be used for nighttime and other periods when the vapor-pressure sampling system was not operated, or for periods when turbulent heat fluxes determined by EBBR were considered unreasonable on the basis of

arguments given by Ohmura (1982). The EBWSP technique requires assumptions about the eddy diffusivities for momentum and heat transport in the surface sublayer that the EBBR technique does not require, and it probably is less desirable than the EBBR technique when reliable measurements of the vapor-pressure gradient are available. The EBWSP technique is not subject to the numerical instabilities that can occur with the EBBR technique when the measured Bowen ratio is close to -1 and it does not require vapor-pressure measurements. For these reasons, the EBWSP technique was a satisfactory means to determine the generally small fraction of the daily latent heat flux that could not be accounted for in this study by the EBBR technique. The EBWSP technique was used to augment the EBBR technique to produce continuous 24-hour records of latent heat flux.

An exception to the above augmentation approach was made when the anemometer used to measure mean windspeed failed. Windspeed is required for the calculation of latent heat flux and evapotranspiration by the EBWSP technique. For periods when the anemometer was faulty, an empirical relation was used to estimate latent heat flux when the EBBR technique could not be used. Regression analysis of 20-minute daytime eddy-correlation and concurrent energy-balance data yielded the statistically significant (r^2=0.92, n=600, P<0.05) relation

$$\lambda E_{ec} = 15.12 + 0.669\, S\frac{R_n - G}{S+\gamma},$$

where

λE_{ec} is latent heat flux from eddy correlation;

S is slope of the saturation vapor-pressure curve evaluated at air temperature at the reference height, in kilopascals per degree Celsius; and

other terms are as previously defined.

For nighttime periods, no statistically significant relation was observed, and nighttime evapotranspiration was neglected when windspeed data were rejected.

The second approach was to calculate evapotranspiration directly from latent heat flux computed using eddy correlation. Because eddy-correlation measurements were performed only intermittently, they were used as an independent check on the more continuous EBBR-EBWSP approach.

Penman Technique for Potential Evapotranspiration

Potential evapotranspiration may be defined as the maximum evapotranspiration that can be sustained from an extensive area densely occupied by active vegetation that is well supplied with water. The concept is useful for estimating evapotranspiration when potential conditions exist. Potential conditions exist when ample moisture is available at the surface. Under such conditions, evapotranspiration is limited by meteorological factors. The Penman equation for potential evapotranspiration (Penman, 1956) can be written (Monteith, 1965)

$$\lambda E_p = \frac{S(R_n - G) + \dfrac{\rho_a C_p (e_s - e)}{r_h}}{(S+\gamma)}, \qquad (16)$$

where

e_s, e are saturation vapor pressure evaluated at air temperature and vapor pressure at the reference height, in kilopascals;

r_h is boundary layer resistance, in seconds per meter; and other terms are as previously defined.

The right side of equation 16 may be broken down into radiation and aerodynamic terms. The term $S(R_n - G) / (S+\gamma)$ is determined largely by net radiation. The term $\rho_a C_p (e_s - e) / (r_h[S+\gamma])$, which is determined by aerodynamic transport, is an indication of atmospheric evaporative demand. The quantity $e_s - e$ is the atmospheric vapor-pressure deficit.

Boundary layer resistance can be calculated from (Campbell, 1977, p. 138)

$$r_h = \frac{\ln\left(\dfrac{[z_w - d + z_h]}{z_h}\right)\ln\left(\dfrac{[z_w - d + z_0]}{z_0}\right)}{k^2 u}, \qquad (17)$$

where

z_h is roughness length for heat transport, in meters; and

other terms are as previously defined.

Instrumentation and measurements used to determine net radiation, subsurface heat flux, and wind speed have been described. Air temperature and vapor pressure were measured at a height of 2.6 m using an air temperature and relative humidity sensor (Model 207, Campbell Scientific, Inc., or Model HMP 35C, Vaisala, Inc.). Vapor pressure was computed as the product of saturation vapor pressure

(Lowe, 1977) and relative humidity. The slope of the saturation vapor-pressure function was evaluated using the equation $S = 5{,}307\ e_s/T_k^2$. Estimation of the roughness parameters d and z_0 has been discussed previously in this report. The roughness length for heat transport was estimated from $z_h = 0.2\ z_0$ (Campbell, 1977, p. 39).

When moisture is limiting to evapotranspiration, calculations of potential evapotranspiration are less useful for estimating actual evapotranspiration because a critical assumption of the potential evapotranspiration concept is that moisture is not limiting. Nonpotential conditions may be said to exist when moisture is limiting. Partitioning of energy at the surface is affected by moisture availability, and this is reflected in the temperature and vapor-pressure profiles that develop near the surface. Air near the surface will likely be warmer and drier during the daytime when nonpotential conditions exist than when potential conditions exist. With this in mind, examination of equation 16 reveals that computed potential evapotranspiration will be larger if the measurements were made under nonpotential rather than potential conditions. Using arguments similar to those of Brutsaert (1982, p. 227), the result from equation 16 can be called "apparent potential evapotranspiration" (E_p' or the latent heat equivalent $\lambda E_p'$). Only under potential conditions does $\lambda E_p' = \lambda E_p = \lambda E$.

Additional micrometeorological measurements.—Total solar radiation was measured using a thermopile-based pyranometer (Model PSP, The Eppley Laboratory, Inc.). Solar radiation was measured every 10 seconds and averaged for 20 minutes. Wind direction was measured every 60 seconds and averaged for 20 minutes using a direction sensor (Model 024A, Met One, Inc.).

Precipitation Measurement

Two different types of precipitation gages were used in this study. The primary gage was a tipping-bucket gage (Model TE525, Texas Electronics, Inc.). That gage, which had a circular, 15.2-cm (6-inch) orifice, was mounted with the orifice above the plant canopy at a height of 1.4 m. The manufacturer indicated the precision of the gage to be about 0.25 mm (0.01 in.). Signals from the tipping-bucket gage were processed and recorded every 20 minutes using a pulse-counting data logger. The tipping-bucket gage was calibrated in the laboratory. Calibration procedures and results are described in the section **"Calibration of a Tipping-Bucket Rain Gage."**

An accumulating precipitation gage was used to provide independent precipitation measurements for comparison with measurements from the tipping-bucket gage and a degree of redundancy in case the tipping-bucket gage failed. The accumulating gage (Catalog number 5-780, Belfort Instrument Co.) had a circular orifice 25.4 mm (10 in.) in diameter. The gage was mounted with the orifice above the plant canopy at a height of 1.2 m. The accumulating gage had a spring-based weighing system to determine precipitation mass and equivalent precipitation depth. Precipitation was recorded as an equivalent depth of water on a battery-powered drum chart. The gage was calibrated using a series of test weights. The mass of each weight was equivalent to that of 25.4 mm of water. A series of mechanical adjustments were made to the weighing system to calibrate the gage. The drum chart was an 8-day chart with 1.3-mm (0.05-inch) graduations. A clock mechanism rotated the drum to record a trace of precipitation with time. There was some play in the clock mechanism and that limited resolution of the time of precipitation to about 2 hours. Typically, the chart was changed during visits made to the site about every 2 weeks to inspect and repair instruments and to measure soil-moisture content. The chart usually revolved more than once between visits. The trace of the recording pen was easily discerned and multiple rotations caused no difficulties in determining daily precipitation. The manufacturer indicated the precision of the gage to be 1.3 mm (0.05 in.). The gage had a total capacity of 305 mm. Precipitation was measured continuously from June 4, 1991, to October 13, 1992.

Calibration of a Tipping-Bucket Rain Gage

Precipitation is typically the largest term in terrestrial water balances and accurate determination of precipitation is needed for quantitative water-balance description. Precipitation measurement errors can occur because a gage does not catch a representative amount of precipitation, or because the gage is not properly calibrated. Catch-related errors can be significant, primarily because of the effects of wind around the gage orifice (Brakensiek and others, 1979); however, proper gage calibration is a prerequisite for accurate determination of precipitation.

Tipping-bucket precipitation gages commonly are used to measure precipitation. Tipping-bucket gages offer several advantages for measuring precipitation, including low initial cost, low maintenance requirements, and compatibility with modern pulse-counting data loggers.

Tipping-bucket gages must be calibrated, and the manner in which the gages operate mechanically can cause the calibration factor to vary with precipitation intensity (Brakensiek and others, 1979). Key functional components of a tipping-bucket gage include a precipitation collector and a precipitation meter. The collector catches precipitation and directs it to one of two equal-capacity reservoirs on the meter. The reservoirs are fixed at opposite ends of a beam with a pivot point in the center. After sufficient precipitation, the mass of the reservoir under the collector becomes great enough to cause the beam to tip. When this happens, the heavier reservoir is emptied and the other reservoir is placed under the collector. During the tip, a magnet on the beam closes a ferrous switch that momentarily completes a circuit that is being monitored by a pulse-counting data logger. Equivalent precipitation for each pulse is computed using a calibration factor. The calibration factor depends principally on the size of the collector orifice and the mass of water required to tip the beam. A finite amount of time elapses between the instant the beam center of mass shifts enough to cause it to tip and the instant the alternate reservoir is positioned under the collector. Water in excess of the amount needed to tip the reservoir is spilled in a quantity dependent on the rate at which it is being delivered by the collector. As a result, the gage calibration factor varies as a function of precipitation intensity. A tipping-bucket rain gage was calibrated under varying intensities of simulated precipitation to examine the effect of precipitation intensity on the calibration factor.

The tipping-bucket gage (Model TE525) was mounted on a tripod with the orifice horizontal. The nominal calibration factor was 0.254 mm (0.01 in.). Water was dripped into the gage by siphoning from a reservoir using small-diameter polyethylene tubing. The inside diameter of the tubing lengths ranged from 0.82 to 1.57 mm, and each was 3.05 m (10 ft) long. The drip rate was varied periodically by changing tubing diameter and height of the reservoir above the gage. The drip rate was measured by collecting water in a weighing pan for a measured period of time and by weighing the water to the nearest 0.001 g on an analytical balance. The mass-basis drip rate (g/h) was converted to simulated precipitation intensity (mm/h) by using the area of the gage orifice and by assuming a density of water of 1.0 g/cm^3. A pulse-counting data logger was used to monitor the gage and compute the reservoir tip rate (h^{-1}). The gage calibration factor was computed from the simulated precipitation intensity divided by the tip rate.

The gage calibration factor was linearly related to the precipitation intensity over the range of 5 to 116 mm/h (P<0.05), indicating that the amount of water spilled during each tip increased as precipitation intensity increased (fig. 3). The effect of increasing intensity was to increase the calibration factor. The regression function predicted the nominal calibration factor of 0.254 mm (0.01 in.) at a precipitation intensity of 52 mm/h. If a gage calibration factor of 0.254 mm was used, the precipitation measurement error would have ranged from 3.6 percent at a precipitation intensity of 5 mm/h to -4.6 percent at a precipitation intensity of 116 mm/h. This analysis indicates that precipitation measurement errors that would result from use of a single calibration factor would vary depending on the precipitation regimen in the field.

When the rain gage was used in the field, the data logger was programmed to apply a correction to account for variation in precipitation intensity. Every 5 minutes, the data logger computed the gage calibration factor based on the measured intensity and

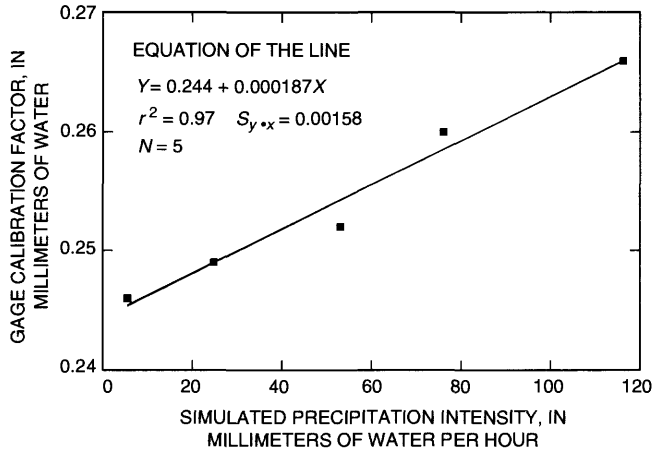

Figure 3. Relation between gage calibration factor and simulated precipitation intensity for a tipping-bucket rain gage.

the regression function given in figure 3. The calibration factor was used to compute a corrected precipitation for the 5-minute period. Precipitation for 5-minute periods was summed for 20 minutes and those values were recorded. Precipitation also was computed using a constant calibration factor (0.254 mm). Both corrected and uncorrected precipitation were recorded in the field from June 16, 1991, to January 16, 1992. Measured precipitation intensity, averaged for 20 minutes, ranged from 0.8 to 78.0 mm/h.

The magnitude of the correction was quite small under the precipitation regimen in the field (fig. 4). Statistical analysis of 20-minute periods indicated that corrected and uncorrected precipitation were not significantly different ($P>0.5$, $n = 337$). The sum of corrected precipitation for the period was 699.7 mm, and that was less than the sum of uncorrected precipitation by less than 1 percent. The slight difference in total precipitation occurred because precipitation was generally less intense than was implied by a calibration factor of 0.254 mm. To the extent that precipitation intensities during the test period were representative of intensities throughout the year, a constant calibration factor of 0.252 mm, which was obtained using the ratio of corrected and uncorrected precipitation for the test period, may provide for slightly more accurate measurement of precipitation catch in that particular gage than will the value 0.254.

Based on the above analysis, reservoir spillage probably was less limiting to gage accuracy in the field than were other factors, such as effects of wind around the gage orifice and limited gage resolution. For example, measurement accuracy for each precipitation event was limited by gage resolution to about 0.25 mm. Because of this limitation, a given precipitation event would have to yield about 125 mm before an error of 0.002 mm in the calibration factor would cause a larger precipitation measurement error than the finite gage resolution.

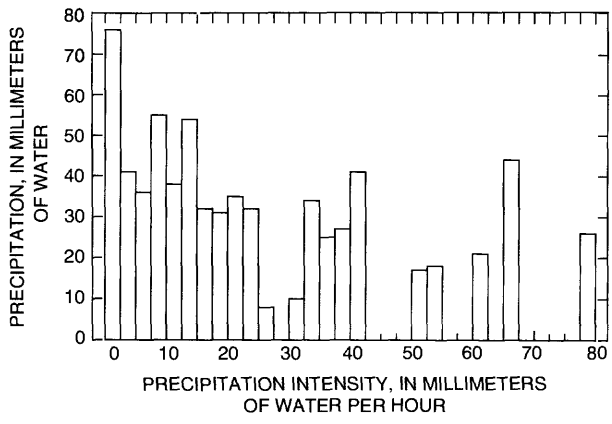

Figure 4. Total precipitation measured at the study site from June 16, 1991, to January 16, 1992, by precipitation intensity class. (The width of each class is 2.5 millimeters per hour.)

Measurement of Soil-Water Content

Volumetric soil-water content was measured using core sampling and the neutron thermalization technique (Gardner, 1986). This technique is based on the phenomenon that high energy neutrons escaping from a radioactive source, such as americium:beryllium, are slowed ("thermalized") principally by collisions with hydrogen nuclei. Because hydrogen is the most effective thermalizer of neutrons in most soils and because most soil hydrogen is associated with water, the relative density of thermalized neutrons is correlated with soil-water content. The neutron moisture gage used in this study was constructed to enable the user to lower an americium:beryllium source and a neutron detector into an access tube buried in the soil. The gage detected and counted thermalized neutrons for a specified duration. The measurement count was divided by a reference count and the resulting count ratio was applied by using a calibration function to determine soil-water content. The calibration function for a neutron moisture gage can vary depending on soil structure and composition, and reliable results are best obtained by calibrating a gage for each soil type in which it is used.

The neutron gage used in this study was calibrated using core samples collected at the field site. The neutron moisture gage (Model 3222, Troxler Laboratories, Inc.) had a 10 mCi source of Am 241:Be. The neutron source and detector were enclosed in a cylindrical, 4.7-cm-diameter probe. Before soil-moisture measurements were made, a 4-minute standard count was obtained while the probe was retracted inside the polyethylene reference standard, an integral part of the gage. Measurement counts were made when the probe was lowered into aluminum access tubes (inside diameter 4.8 cm) buried in the soil. Measurement counts for calibration purposes were accumulated for 4 minutes at each selected depth.

The access tubes were installed in auger holes to depths of 1.2 or 2.1 m, and they protruded approximately 0.15 m above the soil surface. The bottoms of the tubes were sealed with rubber stoppers. The auger holes were slightly larger than the tubes and dry, bagged sand was poured into the space between the tube and the hole wall. The sand was of local origin and it was similar in texture to the soil. The tubes were installed for a minimum of 2 weeks before they were used for measurement.

Two tube installations were sampled destructively to obtain calibration data. First, measurement counts were obtained at the desired depth in each tube. Second, two soil cores (diameter 4.8 cm, length 15.2 cm) were obtained at the probe depth and on opposite sides of the tube using a slide-hammer sampler. The coring was conducted so that depth of each measurement count, as indicated by the ruling on the probe cord, corresponded to the midpoint of the 15.2-cm cores. Depth control for the coring was accomplished by referencing to the top of the access tube. The cores were not maintained intact in the field, but the soil from each core was placed in a steel can that was sealed with electrical tape. Calibration data were obtained from depths of 0.3 and 0.6 m for the first tube in November 1991 and from depths of 0.3, 0.6, and 0.9 m for the second tube in March 1992.

Volumetric water content of each core was computed using the equation

$$\theta = \frac{M_w - M_d}{\rho_w V}, \qquad (18)$$

where

θ is volumetric water content, dimensionless;
M_w is mass of the soil and can before drying, in grams;
M_d is mass of the soil and can after drying, in grams;
ρ_w is density of water, taken to be 1 Mg/m^3; and
V is core volume, in cubic meters.

Soil and cans were weighed, dried at 105°C for 24 to 48 hours, and weighed again to the nearest 0.01 g.

Volumetric water content, averaged between cores taken on opposite sides of the access tubes, was regressed on the count ratio (Gardner, 1986):

$$\theta = a + bf, \qquad (19)$$

where

a, b are regression coefficients, dimensionless; and
f is the ratio of measurement count to the standard count, dimensionless.

Volumetric water content determined by core sampling ranged from 0.09 to 0.30. Little variation was observed between the water contents of cores that were taken from opposite sides of the access tubes at the same depths. The absolute difference between cores in a pair, averaged among all pairs, was 0.006 (standard deviation 0.006). This result indicates that soil-water content and experimental procedures were consistent for each sampling depth and time.

Volumetric water content obtained from core sampling was correlated with the count ratio obtained from the neutron moisture gage (fig. 5). The strength of the relation indicates that soil properties affecting calibration were relatively constant with depth. The negative intercept indicates statistically that the count ratio is greater than zero in dry soil, which is true for soils (Gardner, 1986); however, the relation might not be linear for water contents near zero.

Profiles of volumetric soil-water content were determined approximately every 2 weeks. Water content for the top 0.15 m of soil was routinely sampled using soil cores. The cores were collected from three sites and water content was determined using the equipment and techniques described previously. Volumetric soil-water content below 0.15 m was measured with the neutron moisture gage. Soil-water content was routinely measured at six sites from a depth of 0.3 m to the water table in 0.15-m

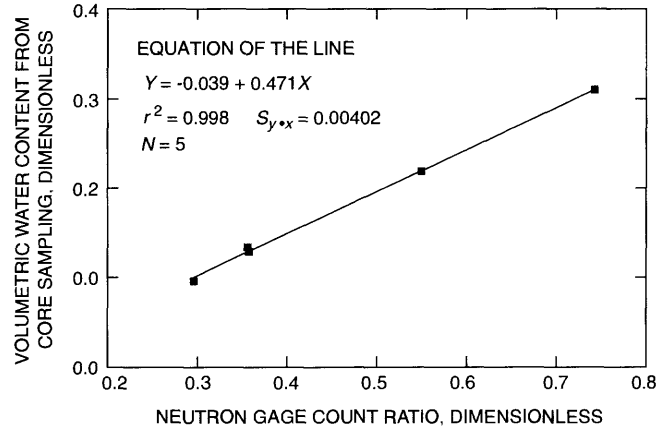

Figure 5. Relation between volumetric soil-water content determined using core samples and the ratio of measurement and standard counts obtained with a neutron moisture gage.

increments. Water content below the water table was not measured routinely; however, measurements were made repeatedly in flooded soil to a depth of 1.7 m. These measurements indicated that water content below the water table varied little from one inundation to the next. The maximum standard deviation, computed from repeated measurements, was 0.02 for the 1.20-m depth. When soil-water content at a given depth in flooded soil was not measured, it was assumed to be equal to the mean value determined in flooded soil at that depth.

Techniques for Estimating Vertical Water Flow

An approach based on Darcy's law was used to estimate vertical drainage (q_d). An equation for steady vertical flux in layered, saturated soil may be written

$$q_d = -\bar{k}_s \frac{\Delta h}{\Delta z} C_v , \qquad (20)$$

where

$\bar{k}_s$ is effective saturated hydraulic conductivity of the soil, in meters per second;

Δz is soil thickness in the vertical direction, in meters;

Δh is hydraulic head difference across the soil thickness, in meters; and

C_v is a factor (8.64×10^7) to convert the flux to millimeters per day, in millimeter seconds per meter day.

Effective saturated hydraulic conductivity ($\bar{k}_s$) in soil can be computed from

$$\bar{k}_s = \frac{\Delta z}{\Sigma \frac{\Delta z_i}{k_{si}}} , \qquad (21)$$

where

Δz_i is thickness of the i^{th} layer, in meters; and

k_{si} is saturated hydraulic conductivity of the i^{th} layer, in meters per second.

In this study, saturated hydraulic conductivity initially was estimated using empirical relations. If soil bulk density and mass fraction of clay and silt are known, Campbell (1985, eq. 12a) predicts saturated hydraulic conductivity (k_s) for a range of soil textures from the equation

$$k_s = 3.9 \times 10^{-5} \left(\frac{1.3}{\rho_b} \right)^{1.3b} \exp(-6.9 m_c - 3.7 m_s) , \qquad (22)$$

where

ρ_b is bulk density, in megagrams per cubic meter;

m_c, m_s are dry mass fractions of clay and silt, dimensionless; and

b is an empirical parameter that can be computed from the mass fractions of sand, silt, and clay, dimensionless.

Equations for b are presented in Campbell (1985, eqs. 2.15 to 2.18 and eqs. 5.10 and 5.11).

Sampling of physical properties of soil to a depth of 6.4 m was conducted at one location near the center of the study area, and at three other locations within about 100 m of the center. Samples were collected in the borehole at approximately 0.7-m intervals using a split-spoon sampler. The sampler was equipped with clear polyvinylchloride (PVC) liners. The split-spoon sampling disturbed the samples. A 0.1- to 0.15-m length of relatively intact sample was removed for analysis. Bulk density was estimated using the computed volume of the liner segment and the oven-dry mass of the intact segment. Finally, samples were sent to a U.S. Geological Survey laboratory for determination of sand, silt, and clay fractions.

Hydraulic head in saturated soil can be computed as the sum of pressure, gravitational, and overburden heads.

$$h = h_p + h_g + h_\Omega$$

where

h_p is pressure head, in meters;

h_g is gravitational head, in meters; and

h_Ω is overburden head, in meters.

The above expression for h neglects effects of solutes. Pressure head arises from hydrostatic or pneumatic forces that can act on the water. Gravitational head arises from the position of the liquid in the gravitational field of the Earth. Overburden head stems from the pressure on the soil matrix that is transferred to the liquid. Spatial hydraulic head differences must be determined in order to compute water flux using equation 20. Hydraulic head differences can be determined using a system of piezometers or monitor wells. A piezometer is a pipe that is open on both ends. One end of the piezometer is placed in saturated soil or sediments to a given depth. The difference in the altitude of the water surface inside neighboring piezometers or monitor wells that are buried to different depths may be used to determine the vertical difference in hydraulic head.

In this study, a system of monitor wells and piezometers was used to determine hydraulic head gradients in the saturated zone and the altitude of the water table (table 2). A set of wells and piezometers was constructed in the center of the study area. The monitor wells, which were constructed of 5-cm inside diameter PVC casing and screen, were installed using 10-cm outside diameter solid-stem augers. The piezometers, which were constructed of 1.6-cm inside-diameter steel pipe, were installed using jetted water. The monitor wells were installed in April 1991 and the piezometers were installed in December 1991. Water levels were measured approximately every 2 weeks using a steel tape. Vertical drainage prior to each set of water-level measurements was assumed to be steady during the period between measurements and equal the value computed from the measurements made at the end of the period. Water level in the center shallow well (W_s) was measured with a pressure transducer (Model PDCR-950, Druck, Inc.) and recorded every 20 minutes. Altitudes of each well or piezometer were established by a traverse of vertical angles from a nearby well for which an altitude had been published (well ID no. 271208082134401; Duerr and Wolansky, 1986).

Computation of the Difference Between Surface-Water and Ground-Water Inflow and Outflow

Measurement techniques that commonly are applied in large-scale basin studies to estimate the contribution of surface-water flows to the water balance could not be used in this study. Because the study area did not constitute a discrete hydrologic catchment, surface-water discharge measurements could not be used to compute the contributions of surface-water flow to the water balance. Although there were no apparent drainage channels at the study site, the potential for sheetflow existed when the water table was above land surface.

The difference between ground-water inflow and outflow for the surficial aquifer was probably small because of the lack of drainage divides and the flat, level nature of the land surface, In another water-balance study, Knisel and others (1985) reported that the difference between ground-water inflow and outflow was negligible for two small watersheds in central Florida. The watersheds studied by Knisel and others (1985) had a much more diverse physiography than the site used in this study, and the potential for divergence of lateral ground-water flows was probably greater.

The difference between surface- and ground-water inflow and outflow was estimated as the residual of the water-balance equation (eq. 1). The sum of the differences was termed "water yield" because it represented the quantity of water that was discharged per unit area per unit time from the study area. Water yield, (q_{ro} - q_{ri} + q_{so} - q_{si}), was computed using the equation

$$q_{ro} - q_{ri} + q_{so} - q_{si} = P - E - \int_0^{D_0} \frac{\partial \theta}{\partial t} dz - qd, \quad (23)$$

where the terms have been described previously.

When the water table was above land surface, computed water yield was composed of the difference between surface-water and ground-water inflow and outflow and the sum of errors in estimates of the remaining water-balance components. When the water table was below land surface, computed water yield was composed of the difference between ground-water inflow and outflow and the sum of errors in estimates of the remaining water-balance components.

Table 2. Identification, relative location, and screened interval of monitor wells and piezometers in the study area

[**Well or piezometer:** Monitor wells are identified with 'W' and piezometers are identified with 'P'. Distance is from the shallow center well (W_s). **Depth interval of well screen:** Interval of depth below the surface for which wells were screened, or depth of piezometer opening]

Well or piezometer	Distance east from W_s (meters)	Distance south from W_s (meters)	Depth interval of well screen (meters)
Ws	0	0	0.3-3.4
W_d	≈2	≈2	5.8-6.1
P_s	≈3	≈1	1.8
P_d	≈3	≈2	3.4

Evapotranspiration and Apparent Potential Evapotranspiration

The approaches used in this study to estimate evapotranspiration rely on measurement of components of the surface energy balance. The surface energy balance is an integral part of the computation of evapotranspiration for the EBBR and

EBWSP techniques and of the computation for potential evapotranspiration. In addition, examination of energy-balance closure is useful for investigating the reliability of evapotranspiration estimated using eddy correlation. The surface energy balance has an important role in estimating evapotranspiration by the micrometeorological methods in this study, and the discussion of evapotranspiration estimates is accompanied by discussion of the surface energy balance.

EBBR-EBWSP Approach

Examples of diurnal energy fluxes during the winter dry and summer wet seasons determined in conjunction with the EBBR-EBWSP approach are shown in figure 6. Diurnal patterns of energy fluxes demonstrated characteristics common to winter and summer periods. Net radiation was nearly zero or negative at night, at dawn, and at dusk. During the daytime, net radiation was strongly correlated with solar radiation. Net radiation increased sharply in the morning, fluctuated during midday, and decreased sharply in the early evening. For analyses in this study, daytime was distinguished from nighttime using measurements of total solar radiation. When measured solar radiation averaged more than 5 W/m^2 for a 20-minute period, the period was designated a daytime period; otherwise, it was considered to be a nighttime period. The small positive value was used as a cutoff, rather than zero, because thermal transients on the thermopile of the pyranometer caused the data loggers to erroneously record a few watts of solar radiation at odd times, such as the middle of the night. Fluctuations in net radiation during midday were caused by clouds that alternately blocked and admitted the solar beam to the land surface. Subsurface heat flux followed patterns similar to net radiation; however, the amplitude of diurnal variation was much less. Subsurface heat flux was significantly correlated with net radiation during the daytime in winter ($r^2 = 0.65$, $P < 0.05$) and summer ($r^2 = 0.95$, $P<0.05$).

Sensible heat flux was nearly zero or negative at night and increased to positive values after net radiation became positive in the morning. In the late afternoon, sensible heat flux decreased to negative values before net radiation became negative. Latent heat flux was nearly zero, negative, or positive at night. Latent heat flux increased sharply with net radiation

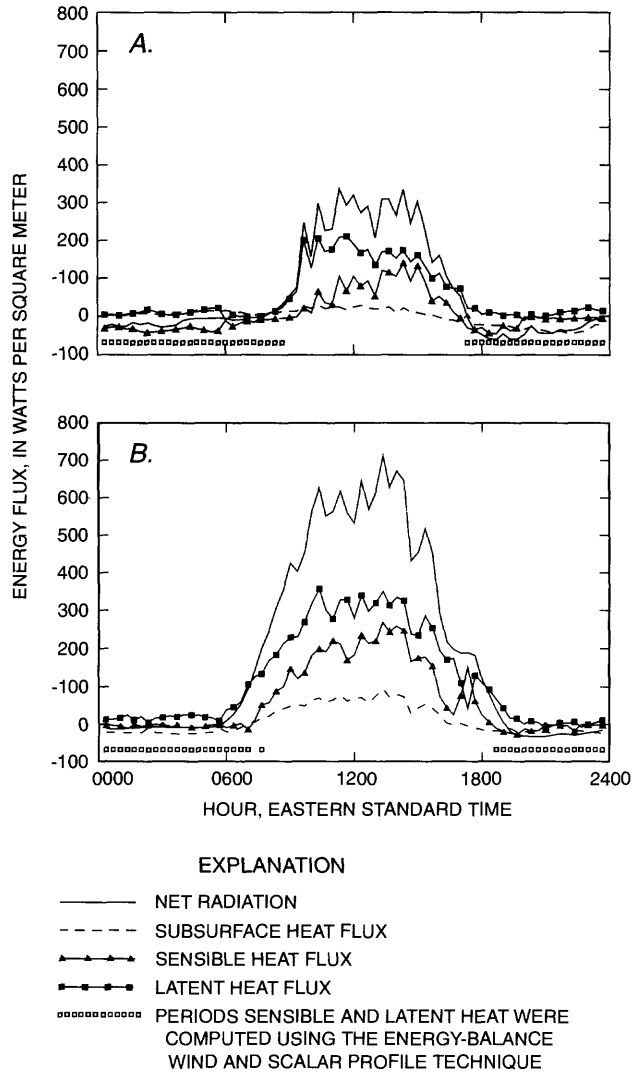

Figure 6. Energy fluxes estimated in conjunction with the energy-balance Bowen ratio and energy-balance wind and scalar profile techniques for (*A*) January 14, 1992, and (*B*) June 19, 1992.

in the morning and decreased sharply with net radiation in the late afternoon. The Bowen ratio was less than 1 during nearly all daytime hours ($\lambda E > H$) for the winter and summer examples, indicating that available energy (R_n-G) was partitioned more to evaporating water than to generating sensible heat.

Diurnal variations of energy fluxes in the examples shown also exhibited differences that were related to season (fig. 6). The most obvious difference was that the amplitude of variations of all four energy fluxes was considerably greater in summer than winter. Incident solar radiation at the field site was greater in summer, and turbulent fluxes

and subsurface heat flux also were higher than they were in winter. Additionally, the sharp morning increase in latent heat flux in the winter example nearly equaled the increase in net radiation, indicating that available energy was decidedly partitioned to evapotranspiration. Winter fog and dew were common at the field site, and the relatively large latent heat flux during the morning of the winter example (fig. 6A) was due to the presence of free water on the vegetation and soil surfaces. Once the free water had been evaporated, partitioning of available energy shifted to generate a greater proportion of sensible heat.

The relative importance of energy-balance terms for computing daily evapotranspiration can best be examined by summing energy fluxes for 24-hour periods (table 3). One of the most obvious effects of averaging energy fluxes for 24-hour periods, rather than daytime periods, is that subsurface heat flux becomes less significant in the surface energy balance. For example, on June 19, subsurface heat flux was 9 percent of net radiation during the daytime, but was only 5 percent of net radiation for the entire 24-hour period. The effect of 24-hour versus daytime averaging on relative importance of subsurface heat flux was even greater on January 14. The reason subsurface heat flux was less important for 24-hour periods is that it was usually negative at night and positive during the day; therefore, the magnitude of total daytime subsurface heat flux was greater than total 24-hour subsurface heat flux.

Seasonal differences are apparent in the two examples shown. Net radiation and sensible and latent heat flux were greater on June 19. Also, the Bowen ratio was higher in June than in January, indicating a greater fraction of available energy was partitioned to evapotranspiration in the winter example. Evapotranspiration was greater on June 19 because total available energy was more than three times greater than on January 14.

In the examples shown (fig. 6), the EBBR techniques could not be used to estimate latent heat flux at night when the vapor-pressure sampling system was turned off. Also, the technique failed to yield physically reasonable energy fluxes during some early and late daytime averaging periods. Ten percent of the daily latent heat flux was computed using the EBWSP technique on January 14 and on June 19.

During the middle of the day, EBBR and EBWSP techniques could be used to determine latent heat flux (fig. 7), and during those periods agreement between the two techniques generally was good. Latent heat flux estimated by the EBWSP technique was slightly higher, but seemed to correlate with latent heat flux determined by the EBBR technique on January 14 ($r^2 = 0.93$) and on June 19 ($r^2 = 0.92$). Results from the two techniques were in good agreement partly because they were not determined independently. Both techniques were applied using the same measured net radiation, subsurface heat flux, and air temperature difference (ΔT).

Summary of EBBR-EBWSP results.—Daily evapotranspiration was computed for June 4, 1991, to October 13, 1992, using the combined EBBR-EBWSP approach (table 4). One measure of the relative contributions of the EBBR and EBWSP techniques in estimating evapotranspiration is the percentage of available energy received during periods when each technique was used. Averaged for the 498 days of field measurement, the EBBR

Table 3. Energy-balance terms estimated in conjunction with energy-balance Bowen ratio and energy-balance wind and scalar profile techniques and summed over 24-hour and daytime periods for the dry prairie study site

[EBBR, energy-balance Bowen ratio; EBWSP energy-balance wind and scalar profile; MJ/m^2•d, megajoules per square meter per day]

Measurement period	Net radiation (MJ/m^2•d)	Subsurface heat flux (MJ/m^2•d)	Bowen ratio	Sensible heat flux (MJ/m^2•d)	Latent heat flux (MJ/m^2•d)
			January 14, 1992		
24-hour	5.38	-0.05	0.14	0.65	4.77
Daytime	6.40	.29	.37	1.65	4.45
			June 19, 1992		
24-hour	16.88	.80	.53	5.56	10.52
Daytime	17.44	1.54	.56	5.74	10.15

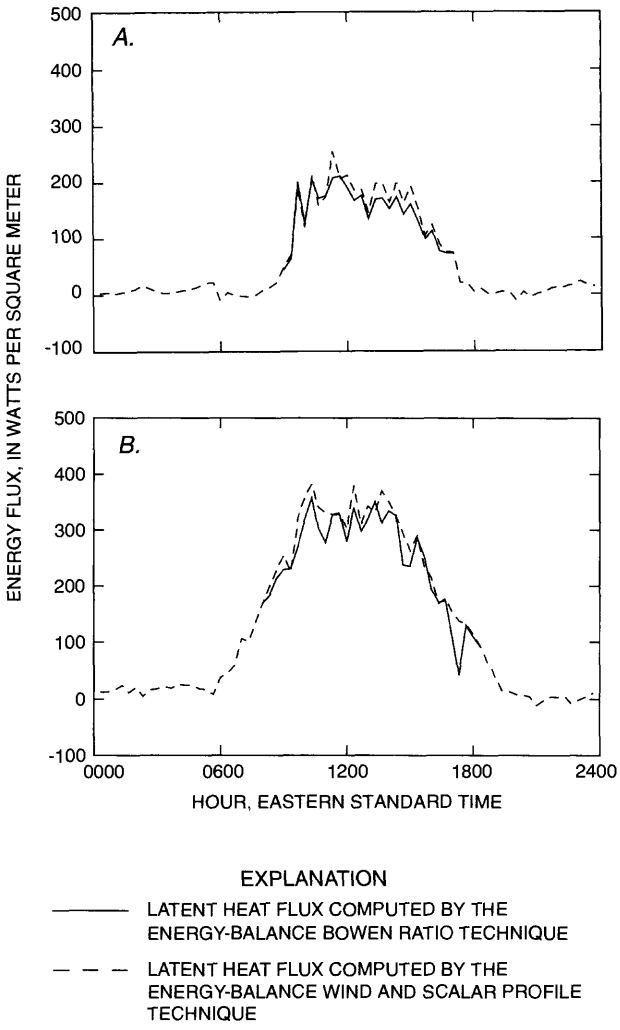

Figure 7. Latent heat flux estimated using the energy-balance Bowen ratio and energy-balance wind and scalar profile techniques for (*A*) January 14, 1992, and (*B*) June 19, 1992.

technique was used during the receipt of 90 percent of the measured available energy. The EBWSP technique was used during 7 percent of the available energy, and 3 percent of the measured available energy occurred during periods when results from both techniques were rejected.

The anemometer used to measure mean wind speed failed completely on August 13, 1991, and it was suspected that it had not worked properly since June 4, 1991. After the anemometer was replaced, only 0.5 percent of the measured available energy occurred during periods when results from both techniques were rejected.

Table 4. Daily equivalent available energy, evapotranspiration, and apparent potential evapotranspiration

[Values are in millimeters per day. Q_e, net radiation minus subsurface heat flux expressed as an equivalent rate of evapotranspiration; E, actual evapotranspiration determined using the techniques energy-balance Bowen ratio and energy-balance wind and scaler profile; E_p', apparent potential evapotranspiration computed using the Penman equation. --, insufficient data]

Date	Q_e	E	E_p'
		1991	
June 4	5.69	3.94	5.85
June 5	4.92	3.71	5.38
June 6	2.79	1.82	2.88
June 7	6.04	3.82	6.23
June 8	5.23	3.65	6.23
June 9	5.25	3.66	6.52
June 10	5.98	4.12	7.08
June 11	6.63	4.42	6.98
June 12	5.07	3.97	4.92
June 13	6.64	4.82	6.77
June 14	6.19	4.29	5.99
June 15	4.75	3.40	4.44
June 16	5.54	4.24	5.24
June 17	4.39	2.83	4.05
June 18	2.65	1.96	2.37
June 19	5.64	4.02	5.61
June 20	5.11	3.82	4.66
June 21	5.98	4.24	5.59
June 22	4.56	3.48	4.07
June 23	4.80	3.66	4.47
June 24	5.34	3.78	4.91
June 25	7.09	3.62	6.35
June 26	5.32	2.86	4.62
June 27	4.80	2.80	4.14
June 28	6.53	4.21	6.24
June 29	6.40	3.68	5.98
June 30	5.81	3.58	5.32
July 1	2.33	1.50	2.35
July 2	3.38	2.40	3.47
July 3	6.02	3.78	5.96
July 4	5.27	3.45	5.34
July 5	5.50	2.96	5.13
July 6	5.24	3.13	5.13
July 7	6.16	3.79	5.91
July 8	6.81	4.41	6.36
July 9	5.57	3.40	5.58
July 10	4.11	2.92	4.33
July 11	2.50	1.81	2.43
July 12	3.81	2.82	3.62
July 13	2.32	1.44	2.36

Table 4. Daily equivalent available energy, evapotranspiration, and apparent potential evapotranspiration—*Continued*

Date	Q_e	E	E'_p	Date	Q_e	E	E'_p
	1991—*Continued*				**1991—*Continued***		
July 14	5.10	3.54	5.00	August 28	4.90	3.06	5.56
July 15	4.44	3.21	4.46	August 29	5.15	3.15	6.02
July 16	5.41	3.32	5.28	August 30	5.33	3.64	5.81
July 17	5.56	3.37	5.59	August 31	5.26	3.51	5.71
July 18	6.57	4.10	6.18	September 1	3.83	2.68	4.15
July 19	5.77	3.17	5.37	September 2	6.09	3.84	6.91
July 20	3.44	2.04	3.19	September 3	4.73	3.14	5.44
July 21	5.97	--	5.71	September 4	4.48	2.98	5.46
July 22	5.77	3.12	5.42	September 5	5.72	3.36	6.10
July 23	6.45	3.29	5.90	September 6	4.87	2.95	5.13
July 24	3.82	2.38	3.52	September 7	5.40	3.61	6.41
July 25	5.16	3.27	4.70	September 8	4.76	3.05	5.84
July 26	4.74	3.47	4.50	September 9	4.88	3.36	5.68
July 27	4.36	2.78	3.88	September 10	5.36	3.44	6.00
July 28	5.10	3.32	4.83	September 11	3.97	2.64	4.16
July 29	4.86	3.26	4.91	September 12	--	--	--
July 30	--	--	--	September 13	--	--	--
July 31	2.62	1.86	2.99	September 14	5.68	3.97	6.28
August 1	4.03	2.94	4.50	September 15	4.98	3.86	6.31
August 2	5.99	3.84	6.39	September 16	4.87	3.34	6.49
August 3	6.53	4.01	6.55	September 17	5.15	3.53	6.33
August 4	6.87	4.22	7.05	September 18	3.97	2.64	4.25
August 5	6.88	3.92	6.90	September 19	5.71	3.58	5.91
August 6	6.46	4.05	6.62	September 20	5.01	3.02	5.20
August 7	5.58	3.67	6.04	September 21	4.03	2.39	4.46
August 8	6.17	4.09	6.25	September 22	5.01	3.05	5.80
August 9	4.10	2.75	4.21	September 23	5.15	2.90	5.61
August 10	5.14	3.37	5.18	September 24	5.26	3.43	5.63
August 11	6.66	4.24	6.86	September 25	4.48	3.47	5.64
August 12	5.98	4.03	6.32	September 26	5.05	3.40	6.27
August 13	6.26	4.10	7.72	September 27	5.81	3.94	7.85
August 14	5.40	3.83	6.71	September 28	4.63	3.45	7.28
August 15	4.84	3.57	5.26	September 29	4.77	3.59	5.97
August 16	6.00	4.02	6.68	September 30	3.64	3.05	5.50
August 17	6.31	4.32	7.88	October 1	1.51	1.39	2.10
August 18	6.37	4.01	7.66	October 2	3.45	2.98	4.29
August 19	4.82	3.41	5.74	October 3	2.39	2.02	2.85
August 20	1.77	1.43	2.20	October 4	3.47	2.65	3.48
August 21	4.71	3.31	5.32	October 5	4.43	3.65	5.27
August 22	2.85	2.00	3.02	October 6	3.54	2.84	3.68
August 23	4.37	2.93	4.71	October 7	3.98	3.50	7.03
August 24	3.51	2.16	3.58	October 8	3.95	2.74	7.45
August 25	5.09	3.29	5.60	October 9	2.80	2.06	4.38
August 26	5.78	3.66	6.34	October 10	3.66	2.44	4.42
August 27	6.39	4.15	7.70	October 11	3.80	2.94	4.32

Table 4. Daily equivalent available energy, evapotranspiration, and apparent potential evapotranspiration—*Continued*

Date	Q_e	E	E'_p
	1991—*Continued*		
October 12	4.63	3.56	5.56
October 13	5.03	3.62	5.42
October 14	4.81	3.69	6.30
October 15	2.40	1.60	2.67
October 16	5.01	3.48	8.55
October 17	5.34	3.96	5.92
October 18	4.76	3.59	6.85
October 19	4.60	2.97	6.04
October 20	4.23	2.83	5.45
October 21	1.63	1.45	2.09
October 22	3.91	2.98	5.79
October 23	3.43	3.18	5.08
October 24	3.92	3.12	6.47
October 25	2.42	2.22	4.12
October 26	3.33	2.91	5.16
October 27	3.87	3.02	4.91
October 28	4.41	3.60	5.43
October 29	3.41	2.80	4.98
October 30	4.18	3.62	7.58
October 31	4.85	3.70	4.88
November 1	4.23	3.38	5.51
November 2	2.23	1.95	2.86
November 3	4.01	2.65	5.54
November 4	2.07	1.52	6.47
November 5	2.25	1.48	4.73
November 6	3.34	1.79	3.94
November 7	2.68	1.56	3.09
November 8	3.74	2.43	6.41
November 9	3.37	2.33	5.68
November 10	3.84	2.12	4.25
November 11	4.46	2.66	6.08
November 12	4.26	2.85	6.02
November 13	4.12	2.72	7.08
November 14	3.64	2.65	4.92
November 15	2.39	1.71	3.33
November 16	3.35	2.42	4.51
November 17	3.05	2.25	4.90
November 18	3.24	2.58	5.37
November 19	2.92	2.49	5.58
November 20	2.06	1.37	3.25
November 21	3.78	2.92	5.61
November 22	3.03	2.15	4.64
November 23	2.82	1.85	3.88
November 24	2.87	2.23	4.32
November 25	3.68	2.01	8.10
November 26	2.34	1.55	5.85
November 27	1.83	1.23	3.58
November 28	2.61	1.95	5.33
November 29	3.02	2.34	5.61
November 30	2.61	1.79	4.61
December 1	2.77	1.66	3.99
December 2	2.76	2.16	4.48
December 3	2.15	1.48	5.14
December 4	1.92	2.09	3.69
December 5	3.11	1.55	5.28
December 6	2.68	2.06	3.90
December 7	2.99	2.29	4.44
December 8	3.19	2.38	4.23
December 9	3.11	2.29	3.46
December 10	3.40	2.35	4.35
December 11	3.09	2.31	3.09
December 12	2.62	.46	3.60
December 13	3.16	2.35	3.79
December 14	2.83	1.98	3.76
December 15	2.80	1.83	6.00
December 16	3.00	2.04	9.71
December 17	3.12	2.27	4.58
December 18	3.31	3.21	3.83
December 19	2.70	2.19	9.85
December 20	2.03	1.91	6.69
December 21	2.76	2.29	4.23
December 22	3.12	2.73	3.57
December 23	3.11	2.18	4.71
December 24	1.79	1.29	2.87
December 25	1.78	1.29	1.97
December 26	1.80	1.09	2.23
December 27	2.16	1.58	3.01
December 28	1.11	.92	2.03
December 29	2.78	1.71	4.07
December 30	3.15	2.16	4.14
December 31	1.91	1.27	2.77
	1992		
January 1	1.37	.89	2.73
January 2	1.86	1.44	2.91
January 3	3.11	2.10	4.96
January 4	2.53	1.56	6.27
January 5	2.82	1.88	2.79
January 6	1.25	1.25	2.02
January 7	3.49	2.14	4.10
January 8	3.44	2.63	5.00
January 9	3.25	2.29	4.92
January 10	1.93	1.55	3.77

Table 4. Daily equivalent available energy, evapotranspiration, and apparent potential evapotranspiration—*Continued*

Date	Q_e	E	E_p'	Date	Q_e	E	E_p'
	1992—*Continued*				1992—*Continued*		
January 11	2.70	1.40	5.64	February 25	1.00	1.36	3.13
January 12	2.49	1.90	4.42	February 26	2.01	1.91	3.72
January 13	1.67	1.29	5.04	February 27	3.59	2.10	5.60
January 14	2.23	1.97	5.07	February 28	4.26	2.42	6.11
January 15	2.45	1.55	3.31	February 29	4.87	3.37	7.47
January 16	2.65	1.27	3.83	March 1	4.80	2.81	5.64
January 17	3.12	1.58	3.44	March 2	4.79	3.62	6.88
January 18	2.70	1.24	4.47	March 3	4.02	2.80	5.87
January 19	.61	.67	1.93	March 4	1.28	1.11	2.04
January 20	3.38	1.72	4.60	March 5	4.47	3.17	7.83
January 21	3.40	2.14	5.43	March 6	4.37	2.82	6.75
January 22	2.64	2.03	6.09	March 7	3.59	2.74	4.35
January 23	1.26	1.21	4.12	March 8	4.92	3.05	6.28
January 24	1.52	1.60	4.00	March 9	5.07	3.07	8.20
January 25	3.61	2.03	4.99	March 10	3.60	1.97	6.64
January 26	3.33	2.07	7.66	March 11	4.24	2.52	5.62
January 27	2.55	1.68	6.49	March 12	1.16	1.01	1.64
January 28	--	--	--	March 13	4.29	2.40	4.76
January 29	3.11	--	4.07	March 14	3.11	2.01	3.94
January 30	2.01	.87	3.85	March 15	5.60	3.12	7.55
January 31	3.16	1.73	5.87	March 16	5.07	2.93	7.01
February 1	4.22	2.77	8.40	March 17	5.23	2.70	6.95
February 2	2.64	1.61	4.24	March 18	4.34	2.34	8.46
February 3	3.70	1.94	4.84	March 19	2.18	1.66	3.63
February 4	3.68	2.01	6.25	March 20	5.57	2.98	9.68
February 5	3.20	2.51	7.70	March 21	5.67	2.99	7.38
February 6	2.50	2.14	5.36	March 22	1.28	1.06	1.33
February 7	3.18	1.87	4.74	March 23	3.43	2.36	4.36
February 8	4.25	2.89	5.75	March 24	5.41	3.17	8.32
February 9	2.90	1.97	4.63	March 25	3.97	2.19	6.13
February 10	3.41	1.97	5.56	March 26	5.77	3.22	8.58
February 11	3.33	1.91	4.43	March 27	5.70	2.70	7.70
February 12	4.27	2.21	4.98	March 28	5.04	2.67	6.21
February 13	3.52	2.38	4.60	March 29	2.95	1.76	4.26
February 14	3.75	2.52	4.85	March 30	5.21	2.83	7.32
February 15	3.93	2.40	7.66	March 31	5.95	3.33	7.20
February 16	2.63	2.07	4.54	April 1	4.79	2.72	5.35
February 17	4.08	2.32	8.13	April 2	5.38	2.97	6.99
February 18	3.88	2.12	7.44	April 3	2.43	1.97	2.93
February 19	3.49	1.60	5.90	April 4	5.85	2.97	7.19
February 20	3.58	2.34	8.43	April 5	5.60	3.00	8.11
February 21	2.43	1.53	7.51	April 6	4.46	2.48	9.18
February 22	2.50	1.43	5.07	April 7	1.02	.83	2.16
February 23	3.49	1.76	7.48	April 8	4.74	2.59	5.58
February 24	2.70	1.44	4.77	April 9	4.81	2.46	6.49

Table 4. Daily equivalent available energy, evapotranspiration, and apparent potential evapotranspiration—*Continued*

Date	Q_e	E	E_p	Date	Q_e	E	E_p
	1992—*Continued*				1992—*Continued*		
April 10	4.99	2.56	6.73	May 25	6.97	3.95	10.28
April 11	3.34	1.90	4.26	May 26	6.69	3.77	9.26
April 12	3.65	2.46	3.81	May 27	6.34	3.05	8.03
April 13	5.92	3.13	8.84	May 28	5.86	3.02	8.50
April 14	5.25	2.82	9.64	May 29	6.77	3.18	10.52
April 15	5.09	3.20	9.45	May 30	4.95	2.81	6.29
April 16	5.08	2.97	9.68	May 31	6.51	3.68	8.42
April 17	5.12	3.12	8.24	June 1	5.81	3.44	7.39
April 18	5.63	3.28	8.49	June 2	4.64	3.29	6.02
April 19	.99	1.04	2.13	June 3	2.16	1.89	3.35
April 20	5.34	3.06	7.52	June 4	5.10	3.07	6.81
April 21	1.57	1.42	2.61	June 5	5.91	3.07	8.26
April 22	4.55	2.70	5.28	June 6	3.53	2.60	3.46
April 23	5.43	2.98	6.30	June 7	3.99	2.60	4.33
April 24	5.38	2.89	6.14	June 8	5.76	3.16	6.34
April 25	5.83	3.00	6.84	June 9	6.37	3.49	7.51
April 26	6.65	3.37	11.45	June 10	5.49	3.15	6.48
April 27	6.76	2.76	12.99	June 11	5.32	3.47	7.20
April 28	6.43	2.47	12.56	June 12	6.74	3.80	8.68
April 29	6.73	2.92	9.97	June 13	4.89	2.90	6.11
April 30	5.59	2.64	7.42	June 14	5.30	3.42	7.05
May 1	5.74	2.74	7.57	June 15	5.44	3.31	5.88
May 2	6.41	3.15	8.40	June 16	4.68	3.00	5.11
May 3	6.50	3.33	9.53	June 17	6.76	3.89	7.98
May 4	6.33	3.51	7.19	June 18	5.96	3.49	7.29
May 5	5.02	3.29	7.65	June 19	6.62	4.31	8.02
May 6	6.10	3.25	9.47	June 20	6.66	3.75	8.83
May 7	4.53	2.31	7.67	June 21	6.20	3.73	8.19
May 8	6.46	2.67	9.67	June 22	6.45	4.10	8.25
May 9	6.29	2.88	7.94	June 23	3.79	2.90	3.79
May 10	6.47	3.18	8.32	June 24	.70	.77	1.11
May 11	6.39	3.37	9.29	June 25	.71	1.02	1.63
May 12	5.75	3.03	7.78	June 26	.66	1.25	1.78
May 13	6.12	3.09	9.34	June 27	4.84	3.17	6.07
May 14	5.66	2.67	7.97	June 28	1.93	1.59	2.42
May 15	5.91	3.15	8.03	June 29	5.50	3.71	6.52
May 16	5.53	2.62	8.88	June 30	6.01	3.94	7.99
May 17	3.13	2.34	4.20	July 1	6.22	4.10	7.97
May 18	5.01	3.18	9.11	July 2	6.18	3.60	7.44
May 19	5.79	3.46	10.40	July 3	6.29	4.02	8.03
May 20	5.96	3.45	11.19	July 4	6.51	3.95	9.41
May 21	5.12	2.56	7.13	July 5	6.17	3.69	7.28
May 22	6.31	3.39	10.94	July 6	6.67	4.13	8.26
May 23	5.94	3.01	8.54	July 7	7.05	4.15	8.75
May 24	6.71	3.40	9.60	July 8	6.53	3.97	7.65

Table 4. Daily equivalent available energy, evapotranspiration, and apparent potential evapotranspiration—*Continued*

Date	Q_e	E	E_p'	Date	Q_e	E	E_p'
	1992—*Continued*				1992—*Continued*		
July 9	6.55	3.79	7.48	August 23	4.98	3.42	7.46
July 10	5.00	3.18	5.96	August 24	1.81	2.46	5.37
July 11	6.18	3.82	6.94	August 25	6.02	3.75	9.47
July 12	4.70	3.16	5.79	August 26	5.77	3.49	7.34
July 13	4.48	3.14	5.03	August 27	6.32	3.60	8.29
July 14	5.38	2.89	5.91	August 28	4.61	2.98	6.54
July 15	5.51	2.90	6.33	August 29	3.93	2.91	4.93
July 16	7.19	4.14	9.26	August 30	4.50	3.23	4.68
July 17	6.98	3.71	8.15	August 31	5.66	3.76	6.78
July 18	4.72	2.69	5.33	September 1	5.49	3.34	6.48
July 19	4.67	2.56	5.14	September 2	5.61	3.73	7.73
July 20	5.43	3.19	6.01	September 3	3.32	2.36	4.00
July 21	5.51	2.97	6.26	September 4	3.52	2.67	4.59
July 22	6.43	3.75	7.68	September 5	5.19	3.60	7.07
July 23	5.96	3.33	7.19	September 6	5.99	3.76	8.43
July 24	5.36	3.34	6.62	September 7	5.45	3.34	7.16
July 25	6.77	4.02	8.35	September 8	5.52	3.36	7.17
July 26	6.42	3.86	7.55	September 9	5.96	3.41	6.85
July 27	6.62	3.82	8.24	September 10	4.96	3.27	6.07
July 28	6.80	4.08	8.97	September 11	4.37	3.23	5.50
July 29	4.96	3.73	6.04	September 12	5.58	3.29	6.71
July 30	4.80	3.24	5.47	September 13	4.89	2.95	6.15
July 31	6.62	4.47	9.08	September 14	4.64	3.26	6.78
August 1	5.57	3.98	6.86	September 15	4.72	3.03	6.11
August 2	5.25	3.18	6.10	September 16	5.18	3.56	6.20
August 3	4.71	3.72	5.24	September 17	5.08	3.54	6.49
August 4	3.84	2.77	4.00	September 18	4.31	2.88	5.51
August 5	4.26	2.68	4.73	September 19	4.74	3.18	5.62
August 6	5.89	3.74	6.77	September 20	3.79	2.39	3.99
August 7	5.04	3.19	6.27	September 21	3.19	2.24	3.99
August 8	5.30	3.46	6.69	September 22	3.42	2.18	4.25
August 9	4.85	3.22	5.41	September 23	3.23	1.94	3.38
August 10	6.26	4.13	7.04	September 24	3.12	1.82	4.47
August 11	5.45	3.48	6.94	September 25	4.78	2.99	7.11
August 12	4.39	2.99	5.77	September 26	4.34	3.03	6.21
August 13	6.50	4.02	9.52	September 27	4.77	3.25	6.53
August 14	5.15	3.72	7.20	September 28	5.50	3.52	7.88
August 15	3.61	2.29	5.11	September 29	4.95	3.20	6.83
August 16	3.46	2.03	4.12	September 30	3.79	2.39	6.45
August 17	4.85	3.38	5.74	October 1	1.39	1.57	4.69
August 18	5.92	3.53	6.78	October 2	.75	1.51	1.96
August 19	5.56	3.41	6.43	October 3	1.95	2.38	5.78
August 20	5.23	3.64	5.93	October 4	4.12	3.27	7.67
August 21	5.56	3.38	7.68	October 5	5.30	3.40	9.41
August 22	5.58	3.22	7.10	October 6	3.55	2.03	5.21

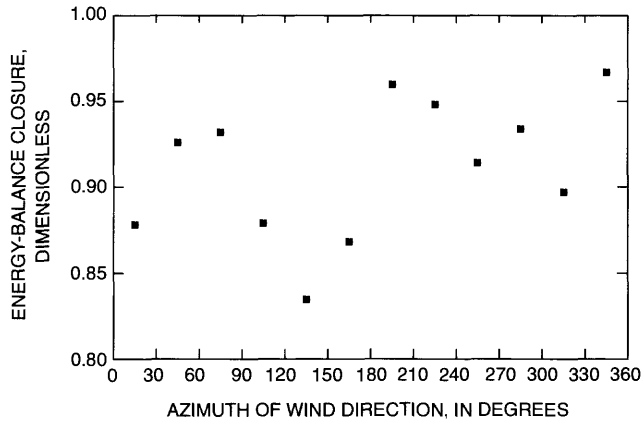

Figure 9. Energy-balance closure observed with eddy-correlation measurements as it varied with wind direction.

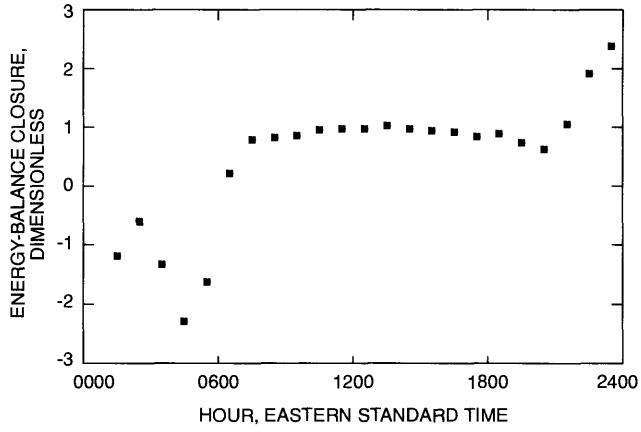

Figure 10. Energy-balance closure observed with eddy-correlation measurements as it varied with time of day.

were not considered. The pattern also could have resulted because the relative importance of individual energy-balance components changed during a 24-hour cycle, and measurement and (or) sampling errors for all components were not equal. For example, a 50-percent error in determining subsurface heat flux (G) during the middle of the day would have little effect on energy-balance closure because that flux is usually much smaller than net radiation, sensible heat flux, and latent heat flux during the day. A 50-percent error in determining subsurface heat flux at night would have a large effect on the computed closure because subsurface heat flux is commonly the term of largest magnitude at night.

The lack of perfect energy-balance closure does cause some uncertainty about the accuracy of evapotranspiration estimates developed using eddy correlation. As has been the case with other studies that have used eddy correlation, it cannot be known which, if any, of the energy-balance component estimates—net radiation, subsurface heat flux, sensible heat flux, or latent heat flux—were principally responsible for the incomplete closure. Energy-balance closure computed in this study generally was closer to the ideal value of 1.0 than has been reported from several other studies in which similar eddy-correlation equipment was used (Weeks and others, 1987; Duell, 1990; Bidlake and others, 1993).

Summary of eddy-correlation results.—Energy fluxes and evapotranspiration computed for 24-hour periods in conjunction with eddy-correlation measurements are shown in table 5. The intermittent eddy-correlation measurements were used to estimate annual evapotranspiration. This was done by the same integration procedure that was described for the EBBR-EBWSP approach. The eddy-correlation data were integrated three times and averaged to obtain a representative annual estimate for the 454-day period during which eddy-correlation measurements were made. The annual estimates ranged from 962 to 976 mm, and the mean estimate was 969 mm.

Comparison of evapotranspiration estimates from eddy correlation and the EBBR-EBWSP approach.—In the absence of independent knowledge of the actual value of evapotranspiration, comparisons of estimates determined by independent techniques are useful for establishing the reliability of the evapotranspiration estimates. Daily evapotranspiration estimates that were obtained using the combined EBBR-EBWSP approach were compared with estimates developed using eddy correlation (fig. 11). The estimates were significantly correlated ($P<0.05$). The slope of the relation was not significantly different from one and the intercept was not significantly different from zero ($P>0.05$), indicating that results of one technique were not biased with respect to the other. In addition, the average daily Bowen ratio ($H/\lambda E$) that was obtained using eddy correlation was significantly correlated with the Bowen ratio estimated using the EBBR-EBWSP approach ($r^2 = 0.56$, n=16, $P<0.05$). The slope of that relation was not significantly different from one and the intercept was not significantly different from zero ($P>0.05$).

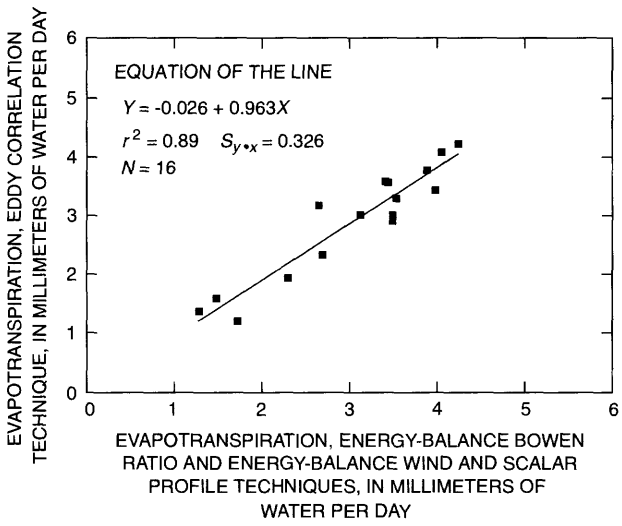

Figure 11. Relation between daily evapotranspiration estimated using eddy correlation and daily evapotranspiration estimated using the energy-balance Bowen ratio and energy-balance wind and scalar profile techniques.

Estimates of annual evapotranspiration computed using eddy correlation and the EBBR-EBWSP approach differed by less than 1 percent. This extremely close agreement probably was fortuitous because the eddy-correlation estimate was based on only 16 days of measurement and the EBBR-EBWSP estimate was based on 492 days.

Evapotranspiration Error

Evapotranspiration estimates developed using the EBBR and EBWSP techniques and eddy correlation are subject to many potential sources of error, and evaluating those sources and quantifying evapotranspiration error are extremely difficult. First, applicability of the three micrometeorological techniques for a given site depends on the propriety of the assumption of a steady-state atmospheric-boundary layer with negligible horizontal gradients of vertical fluxes. No attempt was made in this study to examine the assumption of a steady-state boundary layer; instead, the boundary layer was assumed to be approximately at steady state for the relatively short averaging periods that were used for micrometeorological measurements (20 minutes). No attempt was made in this study to test for horizontal gradients. The assumption of negligible horizontal gradients was based on instrument height and fetch guidelines. Instrument heights in this study and the fetch over fairly uniform vegetation at the study site were sufficient in all directions to meet most published instrument height and fetch guidelines; however, horizontal gradients at the height of the instruments could have resulted in errors in the evapotranspiration estimates.

Second, if atmospheric boundary-layer conditions are met, the problem remains of determining the appropriate time-averaged and space-averaged values for the time-series variables needed to compute evapotranspiration. Measured values of the time-series variables, such as net radiation, subsurface heat flux, vapor-pressure difference, and covariance of vertical wind speed and vapor density, are subject both to random and systematic error. Random error can be random measurement error or the result of inadequate spatial or temporal sampling of the time-series variables. Some components of random error, such as random sampling error, can be estimated using replicated measurements under field conditions; however, the complexity and expense of measuring variables needed for the EBBR, EBWSP, and eddy-correlation techniques generally prohibit extensive replication. Systematic error, or bias, can be a serious source of error for many field measurements. Measurement bias can be the result of imperfect sensor design or improper sensor calibration. Sampling bias can occur because measurements generally are performed at a single fixed location, or at relatively few fixed locations, and the mean of measured values may vary systematically from the scientific true mean (Kempthorne and Allmaras, 1986).

Techniques for evaluating effects of error in the time-series variables on evapotranspiration error for the EBBR technique are presented by Fuchs and Tanner (1970) and by Angus and Watts (1984). Similar error analysis techniques could be devised for the EBWSP and eddy-correlation techniques. The principal challenge to application of evapotranspiration error analysis techniques is estimation of realistic random and systematic error in the field environment. In fact, random and systematic error for many micrometeorological variables, such as net radiation, usually cannot be determined because no reliable standard is available with which to compare the measured values. In a less formal analysis, the uncertainty about the value of a given variable that is determined by two or more independent observations can be described by examining the variability among the observations. In this study, comparisons of independent measurements of some key time-series

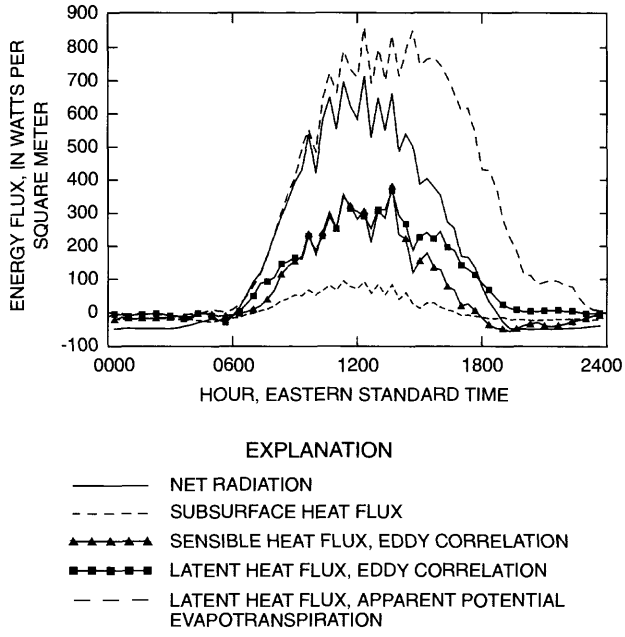

Figure 13. Latent heat flux represented by apparent potential evapotranspiration on May 20, 1992. (Energy fluxes estimated in conjunction with eddy-correlation measurements also are shown.)

representative of actual evapotranspiration. If advected sensible heat had been driving a latent heat flux that was larger than available energy during the afternoon depicted in figure 13, a negative sensible heat flux ($H<0$) would have been detected by eddy correlation; however, eddy-correlation measurements indicated a positive sensible heat flux ($H>0$) during most of the daylight hours.

The unreasonable latent heat flux represented by apparent potential evapotranspiration was caused in part by the aridity of the field site and the persistent regional aridity of the central-Florida dry season. After several weeks without substantial precipitation, average volumetric soil-water content in the uppermost 30 cm, where nearly all plant roots were found, had decreased to about 0.13. Availability of water for latent heat exchange was reduced by senescence of many annual plants and possibly by reduced stomatal conductance in perennials such as saw palmetto. Because of the lack of moisture for latent heat exchange, available energy was partitioned more to sensible heat exchange, as reflected by increased air temperature and atmospheric vapor-pressure deficit near the surface where those time-series variables were monitored. The result was that the aerodynamic term of equation 16 was inflated relative to what it would have been if potential conditions had existed. On a daily basis, the latent heat flux indicated by equation 16 was 27.2 MJ/m^2, which was larger than measured available energy by a factor of 1.9, and the latent heat flux estimated using eddy correlation was 8.7 MJ/m^2.

Annual apparent potential evapotranspiration, which was computed for the period August 13, 1991, to August 12, 1992, was 2,180 mm. This value was greater than annual evapotranspiration estimated using the EBBR-EBWSP approach by a factor of 2.2, and it was about 20 percent greater than the annual potential evapotranspiration reported by Bidlake and others (1993) for a dry prairie site during 1989 and 1990.

Precipitation

Seasonal variation in precipitation during the study, all of which fell as rain, was similar in one respect to seasonal variation in precipitation normals established for 1951-80 at nearby Myakka River State Park (National Oceanic and Atmospheric Administration, 1982). The term "precipitation normal" is used to denote the arithmetic 30-year mean. Monthly precipitation measured in this study and the monthly precipitation normal both indicated a winter dry season and a summer wet season. The 3 months of least precipitation were during winter and the 3 months of greatest precipitation were during summer (fig. 14). Monthly precipitation, however, varied considerably from the corresponding monthly normals. For example, measured precipitation for August 1991 and August 1992 was only 18 percent and 66 percent, respectively, of the August normal. In contrast, precipitation for June 1991 and June 1992

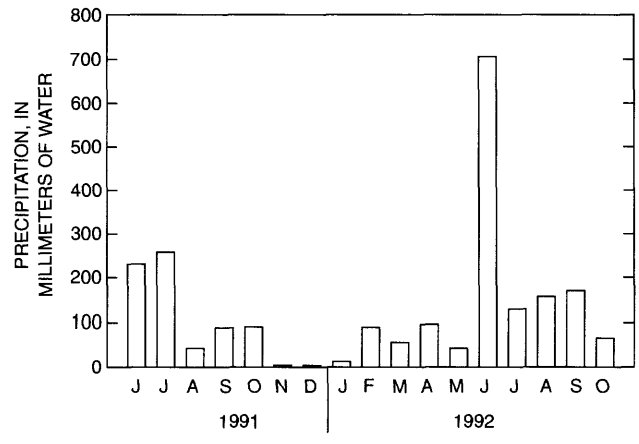

Figure 14. Monthly precipitation at the study site, June 1991 through October 1992.

was 109 percent and 334 percent, respectively, of the June normal. Excluding October 1992, during which time precipitation was measured for only 13 days, variation in the monthly precipitation normal explained only 22 percent of the variation in monthly precipitation.

Total precipitation measured with the tipping-bucket gage for the 498-day period June 4, 1991, to October 13, 1992, was 2,245 mm. Because of the extreme variation in precipitation between 1991 and 1992, precipitation was not integrated multiple times to estimate a representative annual value.

The tipping-bucket and accumulating rain gages were in close agreement when precipitation was summed for periods of several days (fig. 15). Regression analysis indicated that precipitation measured with two gages was strongly correlated ($P< 0.05$), and no relative measurement bias was apparent. The slope of the relation was not significantly different from one and the intercept was not significantly different from zero ($P> 0.05$). The tipping-bucket gage recorded over 580 mm of precipitation during one 4-day period in June 1992. The reservoir of the accumulating rain gage overflowed and data from that period were excluded from the analysis. The limited time resolution of the accumulating rain gage made it difficult to determine daily precipitation when precipitation occurred within about 2 hours of midnight. Because of this, agreement between the gages on a daily basis was not as strong. Effects of limited time resolution were much less pronounced when precipitation was summed for several days.

Agreement between precipitation recorded by the two gages was extremely close when precipitation was summed for the period June 4, 1991, to October 13, 1992. Excluding data from the period when the accumulating rain gage overflowed, the precipitation totals agreed to within 1 percent.

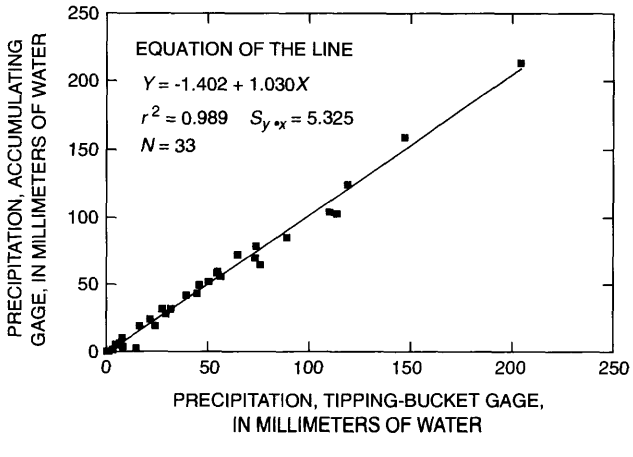

Figure 15. Relation between precipitation measured using an accumulating rain gage and precipitation measured using a tipping-bucket rain gage. (Each data point represents precipitation summed for a period of 8 to 22 days.)

Soil-Water Content and Soil-Water Storage

Typical examples of wet-season and dry-season profiles of soil-water content are shown in figure 16. All measured profiles exhibited the common feature of decreasing water content with depth in the shallowest 0.2 m of soil. Minimum water content generally was reached at depths ranging from 0.3 to 0.8 m, and below that depth water content increased to the bottom of the measured profile. Water-content profiles for the winter dry season differed in some respects from profiles for the summer wet season. The soil was much drier near the surface. This dryness increased more rapidly with depth during the dry season than it did during the wet season.

The soil-water content profiles were integrated with depth to estimate soil-water storage using the equation

$$S_\theta = \sum_{i=1}^{n} \theta_i \Delta z_i , \qquad (24)$$

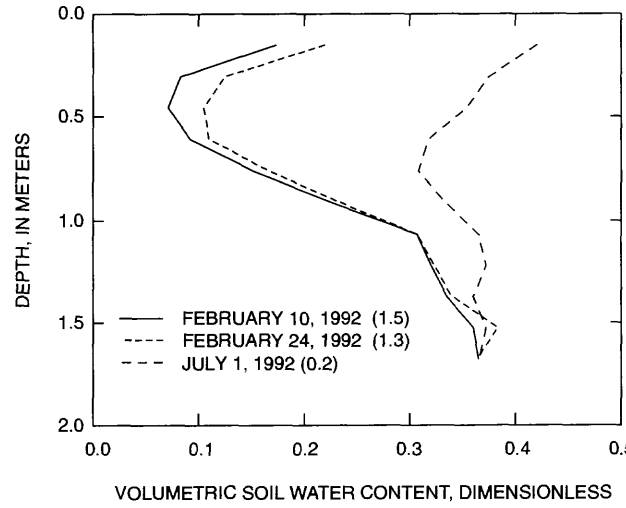

Figure 16. Volumetric soil-water content as it varied with depth on three dates. (Numbers in parentheses indicate depth to the water table, in meters.)

Table 8. Textural and structural characteristics and estimated saturated hydraulic conductivity of soil and sediment samples collected from a single soil profile

[$k_s \times 10^6$: Estimated from Campbell (1985, eq. 6.12a); k_s, saturated hydraulic conductivity; m, meter; Mg/m^3, megagram per cubic meter; m/s, meter per second]

Depth interval (m)	Mass percent			Bulk density (Mg/m^3)	$k_s \times 10^6$ (m/s)
	Sand	Silt	Clay		
1.2-1.8	84.0	6.4	9.6	1.79	4.1
1.8-2.4	82.6	4.0	13.4	1.81	2.5
2.4-3.1	90.0	1.5	8.5	1.85	5.7
3.1-3.7	89.2	1.3	9.5	1.87	4.8
3.7-4.3	91.2	2.4	6.4	1.78	8.4
4.3-4.9	94.1	2.0	4.9	1.83	9.8
4.9-5.5	92.2	1.8	6.1	1.82	8.5
5.5-6.1	.9	31.1	67.9	1.28	.2

conductivity estimated for any other interval (table 8). For steady, one-dimensional flow, the drop in hydraulic head across a flow element is inversely proportional to the effective hydraulic conductivity of the element. The deep monitor well was open to the 5.8- to 6.1-m interval, and vertical differences in hydraulic head that can be inferred from figure 20 probably were the result of an extremely small saturated hydraulic conductivity of sediments of that interval.

Seasonal fluctuations of hydraulic head in the clay could have been due, in part, to changes in overburden head (h_Ω). If the hydraulic conductivity of the clay was small enough, the primary forces acting directly upon the pore water would have been mechanical forces from the clay matrix instead of hydrostatic forces from the column of water above the clay. Seasonal fluctuations in hydraulic head in the clay, then, would have been caused by deformation of the clay matrix due to seasonal loading and unloading of the mass of water in the overlying sands.

Estimates of hydraulic conductivity computed using equation 22 might not have been accurate for all of the samples that were examined. The estimates were likely representative of hydraulic conductivities of the sand and loamy sand samples. Hydraulic conductivity of sand and loamy sand can be expected to range between 10^{-5} to 10^{-6} m/s (Campbell, 1985, table 6.1), and the values for sand samples in table 8 were within that range. The empirical equation given by Campbell (1985, eq. 6.12a), however, may overestimate saturated hydraulic conductivity in soils with such large percentages of silt and clay, as occur in west-central Florida. The estimate developed for the clay sample from the study site could have been as much as two orders of magnitude too large. Measured saturated hydraulic conductivity reported by Stewart and others (1983) for clay samples collected in Hillsborough County ranged from 10^{-9} to 10^{-11} m/s. For example, measured conductivity of one clay sample (26 percent sand, 4 percent silt, 70 percent clay) was 2.2×10^{-11} m/s. Preliminary results from a hydrogeological investigation on the Carlton Reserve indicate hydraulic conductivities for clay on the order of 10^{-9} m/s (G.L. Barr, U.S. Geological Survey, written commun., 1992).

Instead of using equation 22 to compute saturated hydraulic conductivity of the clay, a value of 1.0×10^{-9} m/s was assumed. Saturated hydraulic conductivity of the sand and loamy sand samples was taken from table 8. The computation for effective hydraulic conductivity of the entire profile (eq. 21) strongly reflected the discordant value used for the clay, and for the purpose of estimating vertical flow, the effective hydraulic conductivity of the entire profile was assumed to be equal to the value that was assumed for the clay. Based on the measured differences in hydraulic head and the assumed saturated hydraulic conductivity, maximum computed vertical flow was on the order of 0.01 mm/d. Even if saturated hydraulic conductivity of the clay was assumed to be 10^{-8} m/s, the maximum vertical flux would have been only about 0.1 mm/d. Daily vertical drainage of 0.1 mm/d, summed to a yearly period, would be less than 4 percent of annual evapotranspiration at the site.

NEAR-SURFACE WATER BALANCE

The water balance was integrated for weekly, yearly, and longer periods using average daily water fluxes and average daily rates of soil-water storage. Average daily precipitation, evapotranspiration, and rate of soil-water storage were computed for periods of 8 to 22 days. The daily average rate of soil-water storage was computed from the change in soil-water storage measured at the beginning and end of each averaging period. Precipitation and associated rates of soil-water storage often changed rapidly from one day to the next; however, those components were expressed as daily averages to permit comparisons with evapotranspiration. Because

vertical ground-water flux (q_d) was probably negligible, it was assumed equal to zero and the water-balance equation was solved for the differences between horizontal surface-water and ground-water inflow and outflow, a quantity that is referred to as "water yield" in this report.

The precipitation total of 2,245 mm made it the largest component of the water balance for June 4, 1991, to October 13, 1992 (table 9). Precipitation also was the largest component in the water balance for any one averaging period and varied over a wider range than the other components (fig. 21). Precipitation averaged 42 mm/d during the averaging period of June 16 to July 1, 1992. By contrast, precipitation averaged less than 1 mm/d for 9 of the 34 averaging periods in the study.

Evapotranspiration was the second largest water-balance component for June 4, 1991, to October 13, 1992. Evapotranspiration totaled 63 percent of precipitation for the 498-day period. Maximum average evapotranspiration of about 4 mm/d occurred during the summers (fig. 21). Minimum average evapotranspiration of about 2 mm/d occurred during winter. The transition between summer and winter evapotranspiration was gradual.

Changes in soil-water storage accounted for less than 1 percent of the precipitation during the 498-day period (table 9). Because measurements began after the start of the summer rains in June 1991, when water storage capacity was almost full, and measurements ended near the end of the wet season in October 1992, when soil-water storage capacity was again full, the difference in soil-water storage was small. The average rate of soil-water storage during the study was almost zero, and the apparent contribution of storage to the water balance was negligible for the entire 498-day study period.

Table 9. Components of the site water balance as integrated for different time periods

[All values are in millimeters; *P*, precipitation; *E*, evapotranspiration; ΔS_θ, change in soil-water storage]

Integration period	*P*	*E*	ΔS_θ	Water yield
June 4, 1991, to October 13, 1992	2,245	1,419	19	808
June 4, 1991, to June 2, 1992	1,019	1,000	-197	215
October 9, 1991, to October 13, 1992	1,561	981	41	540

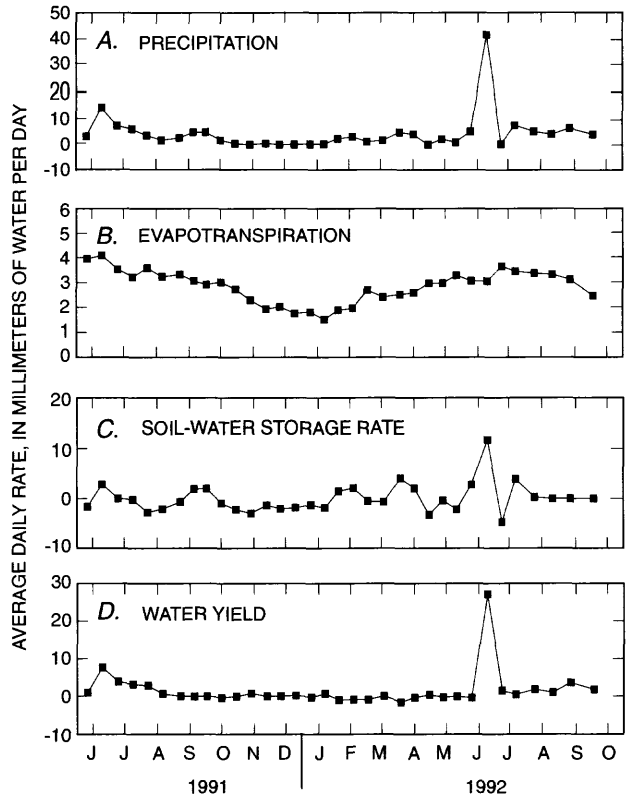

Figure 21. Components of the near-surface water balance. (*A*) Precipitation, (*B*) Evapotranspiration, (*C*) Soil-water storage rate, and (*D*) Water yield. (Each data point represents the mean daily rate from a period of 8 to 22 days.)

Total water yield accounted for 36 percent of precipitation during June 4, 1991, to October 13, 1992 (table 9). Water yield was always less then 1 mm/d and usually less than 0.5 mm/d, except at times during the months of June through August 1991 and during the months of June through October 1992 when the water table was at the surface (fig. 21). Although computed water yield included surface-water and ground-water flow components, the fact that significant yields occurred only when the water table was at the surface might indicate that most of the yield was in the form of surface runoff. Computed water yield was almost zero during the winter and spring months.

Soil-water storage was an important factor in the water balance despite the small mathematical contribution that it made when the water balance was integrated from June 1991 to October 1992. The partitioning of precipitation between evapotranspiration and water yield was largely controlled by the status

SELECTED SERIES OF U.S. GEOLOGICAL SURVEY PUBLICATIONS

Periodical

Preliminary Determination of Epicenters (issued monthly).

Technical Books and Reports

Professional Papers are mainly comprehensive scientific reports of wide and lasting interest and importance to professional scientists and engineers. Included are reports on the results of resource studies and of topographic, hydrologic, and geologic investigations. They also include collections of related papers addressing different aspects of a single scientific topic.

Bulletins contain significant data and interpretations that are of lasting scientific interest but are generally more limited in scope or geographic coverage than Professional Papers. They include the results of resource studies and of geologic and topographic investigations, as well as collections of short papers related to a specific topic.

Water-Supply Papers are comprehensive reports that present significant interpretive results of hydrologic investigations of wide interest to professional geologists, hydrologists, and engineers. The series covers investigations in all phases of hydrology, including hydrogeology, availability of water, quality of water, and use of water.

Circulars present administrative information or important scientific information of wide popular interest in a format designed for distribution at no cost to the public. Information is usually of short-term interest.

Water-Resources Investigations Reports are papers of an interpretive nature made available to the public outside the formal USGS publications series. Copies are reproduced on request unlike formal USGS publications, and they are also available for public inspection at depositories indicated in USGS catalogs.

Open-File Reports include unpublished manuscript reports, maps, and other material that are made available for public consultation at depositories. They are a nonpermanent form of publication that may be cited in other publications as sources of information.

Maps

Geologic Quadrangle Maps are multicolor geologic maps on topographic bases in 7.5- or 15-minute quadrangle formats (scales mainly 1:24,000 or 1:62,500) showing bedrock, surficial, or engineering geology. Maps generally include brief texts; some maps include structure and columnar sections only.

Geophysical Investigations Maps are on topographic or planimetric bases at various scales; they show results of surveys using geophysical techniques, such as gravity, magnetic, seismic, or radioactivity, which reflect subsurface structures that are of economic or geologic significance. Many maps include correlations with the geology.

Miscellaneous Investigations Series Maps are on planimetric or topographic bases of regular and irregular areas at various scales; they present a wide variety of format and subject matter. The series also includes 7.5-minute quadrangle photogeologic maps on planimetric bases that show geology as interpreted from aerial photographs. Series also includes maps of Mars and the Moon.

Coal Investigations Maps are geologic maps on topographic or planimetric bases at various scales showing bedrock or surficial geology, stratigraphy, and structural relations in certain coal-resource areas.

Oil and Gas Investigations Charts show stratigraphic information for certain oil and gas fields and other areas having petroleum potential.

Miscellaneous Field Studies Maps are multicolor or black-and-white maps on topographic or planimetric bases for quadrangle or irregular areas at various scales. Pre-1971 maps show bedrock geology in relation to specific mining or mineral-deposit problems; post-1971 maps are primarily black-and-white maps on various subjects such as environmental studies or wilderness mineral investigations.

Hydrologic Investigations Atlases are multicolored or black-and-white maps on topographic or planimetric bases presenting a wide range of geohydrologic data of both regular and irregular areas; principal scale is 1:24,000, and regional studies are at 1:250,000 scale or smaller.

Catalogs

Permanent catalogs, as well as some others, giving comprehensive listings of U.S. Geological Survey publications are available under the conditions indicated below from the U.S. Geological Survey, Information Services, Box 25286, Federal Center, Denver, CO 80225. (See latest Price and Availability List.)

"Publications of the Geological Survey, 1879–1961" may be purchased by mail and over the counter in paperback book form and as a set of microfiche.

"Publications of the Geological Survey, 1962–1970" may be purchased by mail and over the counter in paperback book form and as a set of microfiche.

"Publications of the U.S. Geological Survey, 1971–1981" may be purchased by mail and over the counter in paperback book form (two volumes, publications listing and index) and as a set of microfiche.

Supplements for 1982, 1983, 1984, 1985, 1986, and for subsequent years since the last permanent catalog may be purchased by mail and over the counter in paperback book form.

State catalogs, "List of U.S. Geological Survey Geologic and Water-Supply Reports and Maps For (State)," may be purchased by mail and over the counter in paperback booklet form only.

"Price and Availability List of U.S. Geological Survey Publications," issued annually, is available free of charge in paperback booklet form only.

Selected copies of a monthly catalog "New Publications of the U.S. Geological Survey" are available free of charge by mail or may be obtained over the counter in paperback booklet form only. Those wishing a free subscription to the monthly catalog "New Publications of the U.S. Geological Survey" should write to the U.S. Geological Survey, 582 National Center, Reston, VA 20192.

Note—Prices of Government publications listed in older catalogs, announcements, and publications may be incorrect. Therefore, the prices charged may differ from the prices in catalogs, announcements, and publications.